



ELSEVIER

Physica D 135 (2000) 263–304

PHYSICA D

www.elsevier.com/locate/physd

## Bursts in oscillatory systems with broken $D_4$ symmetry

Jeff Moehlis\*, Edgar Knobloch

*Department of Physics, University of California at Berkeley, Berkeley, CA 94720, USA*

Received 26 October 1998; received in revised form 10 February 1999; accepted 19 May 1999

Communicated by J.D. Meiss

---

### Abstract

A new mechanism responsible for generating regular and irregular bursts of large dynamic range near onset of an oscillatory instability is identified. The bursts are present in systems with nearly square symmetry and are the result of heteroclinic cycles involving infinite amplitude states created when the square symmetry is broken. All possible cycles of this type are identified and the resulting bursts described. Global connections involving finite amplitude states are also present. The intricate sequence of bifurcations that result is described in several cases. ©2000 Elsevier Science B.V. All rights reserved.

PACS: 47.20.Ky; 05.45.+b; 47.20.-k

Keywords: Bursts; Forced symmetry-breaking; Global bifurcations

---

### 1. Introduction

It has long been known that forced symmetry-breaking, that is, the introduction of small perturbations that reduce the symmetry of a system, can introduce complex dynamics into a system that would otherwise behave in a regular manner [1,2]. From a physics perspective this observation is of particular interest. In physical systems symmetries are rarely exact and some symmetry-breaking imperfections must be assumed to be present. If these imperfections have a dramatic effect on the observed dynamics then studies of idealized symmetric systems appear to have little relevance to the real world. The problem studied in this paper shows that even if this is the case the symmetric system still holds the key for understanding the dynamics in the imperfect system.

Imperfections usually have a dramatic effect precisely in those situations in which the symmetric analysis predicts *no stable* dynamics near onset. These cases are typically deemed to be of little physical relevance and are dismissed. However, symmetry-breaking imperfections can change this situation radically. The Hopf bifurcation with  $O(2)$  symmetry provides a simple example [3]. In this bifurcation two solution branches bifurcate simultaneously from the trivial state at  $\lambda = 0$ ; these correspond to traveling (TW) and standing waves (SW). Among the possible

---

\* Corresponding author  
E-mail address: moehlis@physics.berkeley.edu (J. Moehlis)

bifurcation diagrams that arise is one in which the TW bifurcate subcritically ( $\lambda < 0$ ) and SW supercritically ( $\lambda > 0$ ). Elementary theory [4,5] shows that in this case both branches are unstable near onset. Suppose now that the rotation symmetry is broken but that the reflection symmetry is preserved. Then the SW remain as primary solutions (although they are split into two branches of odd and even parity) and continue to bifurcate supercritically. The TW, however, cannot bifurcate from the trivial solution because of the loss of rotation invariance, and hence *must* bifurcate off one of the SW branches in a *secondary* bifurcation. As a consequence the small amplitude SW are “unmasked” and stable small amplitude states are now present [6]. In this regime Hirschberg and Knobloch [3] find a number of global bifurcations and associated (stable) chaos. In the absence of forced symmetry-breaking the values of  $\lambda$  for which the nontrivial TW and SW states are present do not overlap; consequently no recurrent dynamics are possible. The important consequence of breaking rotation invariance is precisely the generation of a small interval in  $\lambda$  in which both types of solution coexist, thereby allowing connections between them.

In the above example an infinitesimal perturbation of the SW will lead, for  $\lambda > 0$ , to a trajectory that not only escapes to infinity but also looks like a TW at large amplitudes, i.e., there is a connection from a finite amplitude SW to an infinite amplitude TW (cf. [7]). If a mechanism existed for returning the trajectory back to finite amplitude, either in the  $O(2)$ -symmetric problem or in the imperfect problem, a *burst* would result. The absence of such a return mechanism suggests the study of a related problem in which such a mechanism occurs in a natural way. These considerations motivate our study of the Hopf bifurcation with the symmetry of a square. In this system imperfections that break the  $D_4$  symmetry are responsible for the appearance of bursts via a codimension one mechanism. This abstract motivation is complemented by the frequent occurrence of  $D_4$  symmetry in physical systems (see, e.g., [8,9]) and the consequent interest in understanding the role played by symmetry-breaking imperfections in these systems. Moreover, the fact that the resulting bursts can be observed by varying a single parameter makes the present burst generating mechanism of particular relevance to experiments.

The dynamics of the Hopf bifurcation with  $D_4$  symmetry are well understood [10]. In particular it is known that there are several periodic states and in some cases quasiperiodic states as well. Each of these can bifurcate subcritically or supercritically. When the  $D_4$  symmetry is broken a number of homoclinic and heteroclinic connections may be created [11]. Of these the ones of greatest interest are codimension one heteroclinic cycles involving infinite amplitude solutions. Suppose there is a subcritical branch and consider again the regime  $\lambda > 0$ . As in the  $O(2)$ -symmetric Hopf bifurcation a perturbation in the form of the subcritical solutions evolves to infinite amplitude, i.e., for these perturbations the solution “at infinity” is attracting. However, in contrast to the  $O(2)$ -symmetric case, this solution can itself be unstable with respect to perturbations in the form of one of the (unstable) supercritical solutions, thereby providing the required return mechanism and raising the possibility of a heteroclinic cycle between these two solutions. Such a cycle would correspond to a series of infinite amplitude bursts. The period of these bursts will be finite, in contrast to more usual heteroclinic cycles, because the trajectory reaches (and returns from) infinity in finite time. This is the essence of the bursting mechanism explored in this paper. Of course the theory formally breaks down for infinite amplitudes. However, in applications we are interested in bursts of finite amplitude and these are correctly described by the present theory sufficiently close to onset. Because of this restriction the physical amplitude of the bursts is in fact small; what distinguishes them from other dynamical behavior referred to as bursting is their *large* dynamic range [8,9]. In this paper we focus on the burst generation mechanism itself; detailed applications (cf. [11]) are discussed elsewhere [9,12].

The remainder of the paper is organized as follows. In Section 2 we introduce the basic equations describing the Hopf bifurcation with broken  $D_4$  symmetry, and discuss their symmetry properties. In Section 3 we summarize the properties of the perfect  $D_4$ -symmetric system and identify regimes in which heteroclinic cycles to infinity may form. In Section 4 we describe the formation of such cycles when the  $D_4$  symmetry is broken and illustrate the associated dynamics for several particular cases. In addition we identify a number of global bifurcations involving finite amplitude states. The analysis in this section is of necessity largely numerical and forms the bulk of the present

work. In Section 5 we discuss robustness of our results as the magnitude of the symmetry-breaking terms increases and investigate the effects of higher order terms. A number of applications are mentioned in Section 6. Certain aspects of the analysis are relegated to appendices. A brief account of our results has been published elsewhere [12].

## 2. Basic equations and their symmetries

In this paper we study the following (truncated) normal form equations describing a Hopf bifurcation with broken  $D_4$  symmetry:

$$\dot{z}_+ = [\lambda + \Delta\lambda + i(\omega + \Delta\omega)]z_+ + A(|z_+|^2 + |z_-|^2)z_+ + B|z_+|^2z_+ + C\bar{z}_+z_-^2, \tag{1}$$

$$\dot{z}_- = [\lambda - \Delta\lambda + i(\omega - \Delta\omega)]z_- + A(|z_+|^2 + |z_-|^2)z_- + B|z_-|^2z_- + C\bar{z}_-z_+^2. \tag{2}$$

These equations describe the interaction of two nearly degenerate oscillatory modes of opposite parity, with  $z_{\pm}$  denoting the (complex) amplitude of the even/odd modes. The degeneracy is broken by the parameters  $\Delta\lambda$  and  $\Delta\omega$ :  $\Delta\lambda$  measures the difference in the linear growth rates of the two modes and  $\Delta\omega$  the difference between their frequencies at onset. The remaining coefficients are all complex. Under appropriate nondegeneracy conditions (which we assume here) we may neglect all symmetry-breaking contributions to the nonlinear terms. Eqs. (1) and (2) were obtained and partially studied in [11] but are written here using notation that allows us to make contact with earlier work of Swift [10].

When  $\Delta\lambda = \Delta\omega = 0$  Eqs. (1) and (2) have the symmetry  $D_4 \times S^1$ , generated by the three operations

$$\kappa_1 : (z_+, z_-) \rightarrow (z_+, -z_-), \quad \kappa_2 : (z_+, z_-) \rightarrow (z_-, z_+),$$

$$N_{\sigma} : (z_+, z_-) \rightarrow e^{i\sigma}(z_+, z_-), \quad \sigma \in [0, 2\pi].$$

The operations  $\kappa_1, \kappa_2$  generate the group  $D_4$ ; the remaining operation represents the action of the normal form symmetry  $S^1$ . When either  $\Delta\lambda$  or  $\Delta\omega$  are nonzero the symmetry is reduced to  $Z_2 \times S^1$ . Consequently the only primary bifurcations are those to modes of odd or even parity [13]. In addition if  $(z_+, z_-)$  is a nontrivial solution so are the *symmetry-related* solutions  $(-z_+, -z_-)$  and  $(\pm iz_+, \pm iz_-)$ .

In terms of the Swift variables defined by

$$z_+ = r^{1/2} \cos(\theta/2)e^{i(\phi+\psi)/2}, \quad z_- = r^{1/2} \sin(\theta/2)e^{i(-\phi+\psi)/2},$$

and a new time  $\tau$  defined by  $d\tau/dt = r$ , Eqs. (1) and (2) take the more convenient form

$$\frac{dr}{d\tau} = 2(\lambda + \Delta\lambda \cos \theta) + r[2A_R + B_R(1 + \cos^2 \theta) + C_R \sin^2 \theta \cos 2\phi], \tag{3}$$

$$\frac{d\theta}{d\tau} = \sin \theta[\cos \theta(-B_R + C_R \cos 2\phi) - C_I \sin 2\phi] - \frac{2}{r} \Delta\lambda \sin \theta, \tag{4}$$

$$\frac{d\phi}{d\tau} = \cos \theta(B_I - C_I \cos 2\phi) - C_R \sin 2\phi + \frac{2}{r} \Delta\omega, \tag{5}$$

$$\frac{d\psi}{d\tau} = 2A_I + B_I + C_I \cos 2\phi + C_R \sin 2\phi \cos \theta + \frac{2\omega}{r}, \tag{6}$$

where  $A = A_R + iA_I$ , etc. It will also sometimes be useful to consider the  $(u, v, w)$  coordinates defined by

$$u + iv = r \sin \theta e^{i\phi} = 2z_+ \bar{z}_-, \quad w = r \cos \theta = |z_+|^2 - |z_-|^2, \quad e^{i\psi} = \frac{z_+ z_-}{|z_+ z_-|}.$$

In these coordinates, Eqs. (1) and (2) become

$$\frac{du}{dt} = 2\lambda u - 2\Delta\omega v + (2A_R + B_R + C_R)ru - (B_I + C_I)vw, \quad (7)$$

$$\frac{dv}{dt} = 2\lambda v + 2\Delta\omega u + (2A_R + B_R - C_R)rv + (B_I - C_I)uw, \quad (8)$$

$$\frac{dw}{dt} = 2\Delta\lambda r + 2\lambda w + 2(A_R + B_R)rw + 2C_Iuv, \quad (9)$$

$$\frac{d\psi}{dt} = 2\omega + r \left( 2A_I + B_I + C_I \frac{u^2 - v^2}{u^2 + v^2} + 2C_R \frac{uvw}{r(u^2 + v^2)} \right). \quad (10)$$

As a consequence of the  $S^1$  symmetry of Eqs. (1) and (2) the variable  $\psi$  decouples in both cases. In the following we refer to the equivalent sets of Eqs. (3)–(5), and (7)–(9) as the *three-dimensional* system. Since  $\psi$  (modulo  $4\pi$ ) is periodic in time both for fixed points and periodic solutions of the three-dimensional system such solutions in fact correspond to periodic solutions and tori in the original four-dimensional system (1) and (2). The invariance of the system (3)–(5) with respect to reflections in the plane  $\theta = \pi$  and the translations  $\theta \rightarrow \theta + 2\pi$ ,  $\phi \rightarrow \phi + \pi$  enables us to restrict the variables  $(\theta, \phi, \psi)$  to the intervals  $0 \leq \theta < \pi$ ,  $0 \leq \phi < \pi$ ,  $0 \leq \psi < 4\pi$ . These symmetries imply that if  $(r, \theta, \phi)$  is a solution of Eqs. (3)–(5) so are  $(r, 2\pi - \theta, \phi)$  and  $(r, \theta + 2m\pi, \phi + n\pi)$ . Here  $m$  and  $n$  are integers. However, since the restriction  $0 \leq \phi < \pi$  identifies symmetry-related solutions with distinct physical manifestations (for example, winking states with bursts localized on the left or right side of the container would be identified, cf. [12]), we continue using the range  $-2\pi \leq \phi < 2\pi$ . In the  $(u, v, w)$  variables,

$$\kappa_1 : (u, v, w) \rightarrow (-u, -v, w).$$

Thus, if  $(u_0, v_0, w_0)$  is a solution of Eqs. (7)–(9) so is  $(-u_0, -v_0, w_0)$ . Consequently a solution that is not invariant under  $\kappa_1$  will have a  $\kappa_1$ -related counterpart. In the following we use  $r = |z_+|^2 + |z_-|^2 = \sqrt{u^2 + v^2 + w^2}$  as a useful measure of the amplitude of the perturbation from the trivial state.

Eqs. (1) and (2) also have additional symmetries called parameter symmetries. For a parametrized family of ODEs given by  $\dot{X} = f(X, \Lambda)$ , Swift [10] defines a *parameter symmetry* as a symmetry of the extended system  $\dot{X} = f(X, \Lambda)$ ,  $\dot{\Lambda} = 0$  such that

$$f(\gamma_x X, \gamma_\Lambda \Lambda) = \gamma_x f(X, \Lambda),$$

where  $\gamma_x$  is a group action on the phase space variables and  $\gamma_\Lambda$  is a group action on the parameters. This is to be distinguished from a *true symmetry* in which the group acts only on the phase space variables. The parameter symmetries are most easily given in the  $(u, v, w, \psi)$  variables; it is readily verified that the following group actions are parameter symmetries of Eqs. (7)–(10):

$$P_2 : (u, v, w, \psi) \rightarrow (-v, -u, -w, \psi)$$

$$(A, B, C, \lambda, \omega, \Delta\lambda, \Delta\omega) \rightarrow (A, B, -C, \lambda, \omega, -\Delta\lambda, -\Delta\omega),$$

$$P_3 : (u, v, w, \psi) \rightarrow (u, v, w, \psi)$$

$$(A, B, C, \lambda, \omega, \Delta\lambda, \Delta\omega; t) \rightarrow (-A, -B, -C, -\lambda, -\omega, -\Delta\lambda, -\Delta\omega; -t),$$

$$P_4 : (u, v, w, \psi) \rightarrow (-u, -v, -w, -\psi)$$

$$(A, B, C, \lambda, \omega, \Delta\lambda, \Delta\omega) \rightarrow (\bar{A}, \bar{B}, \bar{C}, \lambda, -\omega, -\Delta\lambda, \Delta\omega).$$

If  $\Delta\lambda = \Delta\omega = 0$  and we restrict attention to the reduced phase space  $(u, v, w)$  an additional parameter symmetry is present:

$$P_1 : (u, v, w) \rightarrow (v, w, u)$$

$$(A, B, C, \lambda) \rightarrow \left( A + B - C, -\frac{1}{2}B + \frac{3}{2}C, -\frac{1}{2}B - \frac{1}{2}C, \lambda \right).$$

This symmetry is relevant to the *perfect* system,  $\Delta\lambda = \Delta\omega = 0$ , only.

### 3. The perfect system ( $\Delta\lambda = \Delta\omega = 0$ )

When the  $D_4$  symmetry is exact ( $\Delta\lambda = \Delta\omega = 0$ ) Eqs. (4) and (5) for  $\theta(\tau)$  and  $\phi(\tau)$  decouple from the others. We may think of this two-dimensional system as describing dynamics on the surface of a *sphere* of variable radius  $r(\tau)$  and refer to it, following Swift [10], as the associated spherical system. The radius  $r(\tau)$  corresponding to a given solution of this system can be found by integrating the  $r$ -equation evaluated on this solution. The fixed points  $(\theta_0, \phi_0)$  of the associated spherical system are summarized in Table 1 and correspond to periodic solutions to Eqs. (1) and (2). The isotropy subgroup is the set of group elements of  $D_4 \times S^1$  which act as the identity on the solution. This table also summarizes the terminology we shall use to refer to the various solutions and defines the  $u, v$  and  $w$  fixed points in both sets of variables. Their amplitude  $r(\lambda)$  is given by

$$r = -\frac{2\lambda}{F(\theta_0, \phi_0)} > 0,$$

where

$$F(\theta, \phi) = 2A_R + B_R(1 + \cos^2\theta) + C_R \sin^2\theta \cos 2\phi.$$

Thus, if  $F(\theta_0, \phi_0) < 0$  the fixed point branch bifurcates supercritically, while if  $F(\theta_0, \phi_0) > 0$  the branch bifurcates subcritically.

Swift also proved that in open regions of parameter space there exists a periodic orbit  $(\theta^*(\tau), \phi^*(\tau))$  in the associated spherical system corresponding to a quasiperiodic solution (hereafter  $qp$ ) to Eqs. (1) and (2). The  $qp$  branch bifurcates supercritically from the trivial state if  $\bar{F} < 0$  and subcritically if  $\bar{F} > 0$ , where

$$\bar{F} = \frac{1}{T_\tau} \int_0^{T_\tau} F(\theta^*(\tau'), \phi^*(\tau')) d\tau'$$

Table 1

Fixed point solutions in the associated spherical system for the perfect system ( $\Delta\lambda = \Delta\omega = 0$ ). The  $ns$  solutions only exist in the open regions of parameter space defined by  $|B|^2 > |C|^2$ ,  $|C|^2 > |\text{Re}(B\bar{C})|$ , and their form in the  $(u, v, w)$  variables is omitted. The isotropy subgroup is given in terms of its action on the  $(u, v, w)$  space; the element  $(\kappa_2\kappa_1)^2$  which acts as the identity on this space is omitted.

Name	Isotropy subgroup	$(\theta_0, \phi_0)$	$(u_0, v_0, w_0)$
$u$ solution	$\langle \kappa_2 \rangle$	$\cos \theta_0 = 0$ $\cos 2\phi_0 = 1$	$v_0 = w_0 = 0$
$v$ solution	$\langle \kappa_2\kappa_1 \rangle$	$\cos \theta_0 = 0$ $\cos 2\phi_0 = -1$	$u_0 = w_0 = 0$
$w$ solution	$\langle \kappa_1 \rangle$	$\sin \theta_0 = 0$	$u_0 = v_0 = 0$
$ns$ solution	Id	$\sin^2 \theta_0 = \frac{ C ^2( B ^2 -  C ^2)}{ B ^2 C ^2 - [\text{Re}(B\bar{C})]^2}$ $\cos 2\phi_0 = \frac{\text{Re}(B\bar{C})}{ C ^2}$	

Table 2

Eigenvalues for fixed point solutions of the three-dimensional system Eqs. (3)–(5) for the perfect problem. The radial eigenvalue  $s_1$  is the amplitude eigenvalue and corresponds to perturbations with no component in the  $\theta$  or  $\phi$  direction, while the angular eigenvalues  $s_2$  and  $s_3$  correspond to perturbations in the associated spherical system. The radial eigenvalue for a fixed point with  $(\theta, \phi) = (\theta_0, \phi_0)$  is  $F(\theta_0, \phi_0)$ , so if the radial eigenvalue is positive (negative) the branch bifurcates subcritically (supercritically). The  $ns$  fixed points are always saddles in the associated spherical system; thus  $s_2^{ns} s_3^{ns} < 0$  [10]. The expressions for the determinants in the lower table on p. 361 of [10] are all too small by a factor of 2.

Solution	Eigenvalues
$u$	$s_1^u \equiv 2A_R + B_R + C_R$ $\{s_2^u, s_3^u\}: s_2^u + s_3^u = B_R - 3C_R$ $s_2^u s_3^u = 2(C_R^2 + C_1^2 - B_R C_R - B_1 C_1)$
$v$	$s_1^v \equiv 2A_R + B_R - C_R$ $\{s_2^v, s_3^v\}: s_2^v + s_3^v = B_R + 3C_R$ $s_2^v s_3^v = 2(C_R^2 + C_1^2 + B_R C_R + B_1 C_1)$
$w$	$s_1^w \equiv 2(A_R + B_R)$ $\{s_2^w, s_3^w\}: s_2^w + s_3^w = -2B_R$ $s_2^w s_3^w =  B ^2 -  C ^2$
$ns$	$s_1^{ns} \equiv 2A_R + \frac{B_R [  C ^2 ( B ^2 +  C ^2) - 2(\text{Re}(B\bar{C}))^2 ] + C_R ( B ^2 -  C ^2) \text{Re}(B\bar{C})}{ B ^2  C ^2 - (\text{Re}(B\bar{C}))^2}$

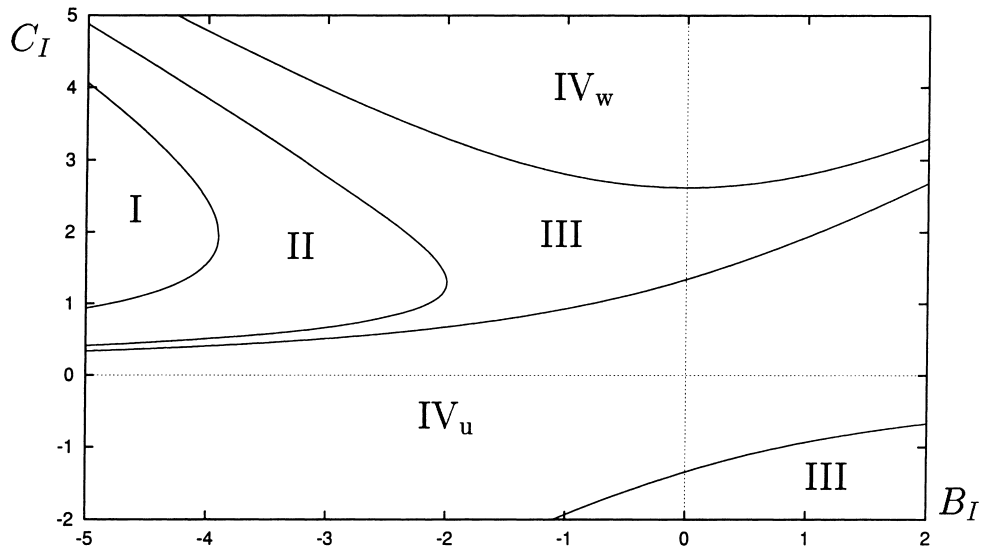


Fig. 1. Distinct regions of parameter space with  $B_R = -2.8$  and  $C_R = -1$ . The boundaries between regions I and II (given by  $s_2^v s_3^v = 0$ ), III and IV<sub>w</sub> (given by  $s_2^w s_3^w = 0$ ), and III and IV<sub>u</sub> (given by  $s_2^u s_3^u = 0$ ) correspond to the condition for a pitchfork bifurcation of the  $v$ ,  $w$ , and  $u$  fixed points, respectively; this bifurcation leads to the creation or destruction of  $ns$  solutions which exist only in regions II and III. The boundary between regions II and III corresponds to the condition that a heteroclinic orbit connecting two  $ns$  solutions forms, creating or destroying the  $qp$  solutions; the location of this boundary must be found numerically. Similar regions of parameter space exist for other values of  $B_R$  in the range  $-3 < B_R < -1$  with  $C_R = -1$ .

and  $T_\tau$  is the period of the orbit (cf. [14]), and can take the form of either a *libration* (where after one period the variable  $\phi$  returns to its original value) or a *rotation* (where after one period the variable  $\phi$  increases by a nonzero multiple of  $\pi$ ) [15].

Table 2 summarizes the linear stability properties of the fixed point solutions of the three-dimensional system (3)–(5); note that in these equations the time  $\tau$  is used. The branches are radially stable (unstable) if they bifurcate

Table 3

Existence and angular stability properties of all solutions for  $-3 < B_R < -1$  and  $C_R = -1$ . For given parameters the region is determined by the values of  $B_I$  and  $C_I$  (see Fig. 1). In this parameter range the  $qp$  solutions are attracting if they exist and hence are sinks within the associated spherical system.

Region	Solution	Properties
I	$u$	Source
	$v$	Saddle
	$w$	Source
	$ns$	Absent
	$qp$	Sink
II	$u$	Source
	$v$	Sink
	$w$	Source
	$ns$	Saddle
	$qp$	Sink
III	$u$	Source
	$v$	Sink
	$w$	Source
	$ns$	Saddle
	$qp$	Absent
IV <sub>w</sub>	$u$	Source
	$v$	Sink
	$w$	Saddle
	$ns$	Absent
	$qp$	Absent
IV <sub>u</sub>	$u$	Saddle
	$v$	Sink
	$w$	Source
	$ns$	Absent
	$qp$	Absent

supercritically (subcritically) from the trivial state. The dependence of the angular eigenvalues of the solutions on parameters can be simplified using the parameter symmetries and rescaling time to restrict attention to the parameter range

$$-3 < B_R < -1, \quad C_R = -1.$$

We may also restrict attention to the case  $B_I < 0$ . Appendix A describes how to deduce the properties of solutions for parameters which do not lie within this range. Note that the parameter symmetry can change a libration to a rotation and vice versa. For fixed  $B_R$  and  $C_R$  the  $(B_I, C_I)$  plane may be divided into distinct regions (see Fig. 1); the stability properties of the solutions in these regions are summarized in Table 3; typical phase portraits are shown in Fig. 12 of [10]. As  $B_R \rightarrow C_R$  the  $qp$  solution may approach a heteroclinic orbit connecting a pair of symmetry-related  $v$  fixed points (see Table 4), and as  $B_R \rightarrow 3C_R$  the  $qp$  solution approaches a  $u$  solution, with a Hopf bifurcation occurring at  $B_R = 3C_R$ . The dependence of the radial stability on parameters for the  $u$ ,  $v$ , and  $w$  solutions may be easily deduced from the radial eigenvalues in Table 2; the resulting possibilities are shown in Fig. 5 of [10]. The radial stability of the  $ns$  and  $qp$  solutions is not discussed in [10] but may be understood through a combination of analytical and numerical arguments, a summary of which appears in Appendix B. A useful observation is that  $A_R$  may be thought of as controlling the radial stability of the solutions: as  $A_R$  increases with all other parameters held fixed it becomes more likely for any of the solutions to be subcritical.

Table 4

Conditions for existence and stability of heteroclinic orbits in the associated spherical system connecting pairs of  $u$ ,  $v$  and  $w$  fixed points, obtained by applying parameter symmetries to the results of [10]

Fixed points	Conditions for existence	Condition for angular stability
$u$	$B_R + C_R = 0$ $ C ^2 - B_R C_R - B_I C_I < 0$ $ -\frac{1}{2}B_I + \frac{3}{2}C_I  <  \frac{1}{2}B_I + \frac{1}{2}C_I $	$B_R - 3C_R < 0$
$v$	$B_R - C_R = 0$ $ C ^2 + B_R C_R + B_I C_I < 0$ $ \frac{1}{2}B_I + \frac{3}{2}C_I  <  \frac{1}{2}B_I - \frac{1}{2}C_I $	$B_R + 3C_R < 0$
$w$	$C_R = 0$ $ B_I  <  C_I $ $ B ^2 <  C ^2$	$B_R > 0$

#### 4. Bursts in the imperfect system ( $\Delta\lambda \neq 0$ , $\Delta\omega \neq 0$ )

##### 4.1. Burst mechanism

Because the associated spherical system (4) and (5) is two-dimensional when  $\Delta\lambda = \Delta\omega = 0$  no complex dynamics are possible in the perfect system unless the  $S^1$  normal form symmetry is broken as in the Faraday system [16,17]. We do not pursue this possibility here, and instead focus on the effects of breaking the  $D_4$  symmetry; as shown numerically in [11] this leads to the possibility of bursts for certain parameter values. Here we will elucidate the mechanism by which these bursts occur.

For the equations with broken  $D_4$  symmetry ( $\Delta\lambda \neq 0$  and/or  $\Delta\omega \neq 0$ ) only the fixed points with even and odd parity remain as primary branches; these are the analogs of the  $w$  fixed points for the three-dimensional perfect system and are given by [11]

1.  $w_e$  solution (even)

$$u = v = 0, \quad r = w = \frac{-\lambda - \Delta\lambda}{A_R + B_R}; \quad \theta = 0, \quad (11)$$

2.  $w_o$  solution (odd)

$$u = v = 0, \quad r = -w = \frac{-\lambda + \Delta\lambda}{A_R + B_R}; \quad \theta = \pi. \quad (12)$$

These solutions only exist for  $r > 0$ . The analogs of the remaining primary branches may bifurcate in secondary bifurcations from these or they may form disconnected branches; they are most easily found numerically.

To make the large amplitude behavior associated with bursts more manageable we let  $\rho = 1/r$  in Eqs. (3)–(5), giving

$$\frac{d\rho}{d\tau} = -\rho[2A_R + B_R(1 + \cos^2\theta) + C_R \sin^2\theta \cos 2\phi] - 2(\lambda + \Delta\lambda \cos\theta)\rho^2, \quad (13)$$

$$\frac{d\theta}{d\tau} = \sin\theta[\cos\theta(-B_R + C_R \cos 2\phi) - C_I \sin 2\phi] - 2\Delta\lambda \sin\theta\rho, \quad (14)$$

$$\frac{d\phi}{d\tau} = \cos\theta(B_I - C_I \cos 2\phi) - C_R \sin 2\phi + 2\Delta\omega\rho. \quad (15)$$

These equations have an important *invariant* subspace  $\Sigma \equiv \{(\rho, \theta, \phi) | \rho = 0\}$  corresponding to *infinite* amplitude states. The invariance of this subspace lies at the heart of the bursting mechanism described below. In this subspace Eqs. (14) and (15) reduce to Eqs. (4) and (5) with  $\Delta\lambda = \Delta\omega = 0$ , i.e., to the perfect system. Thus the fixed points, limit cycles and heteroclinic orbits in the associated spherical system that governs the dynamics of the perfect system continue to exert significant effect on all large amplitude states of the imperfect system, and it is in this sense that the perfect system organizes the dynamics of the imperfect one. In the following we label the infinite amplitude fixed points by analogy to the (finite amplitude) fixed points for the perfect problem; for example,  $u_\infty$  fixed points have  $\rho = 0$ ,  $\cos\theta = 0$ ,  $\cos 2\phi = 1$ , etc.

Because of the above relation between the two systems the angular eigenvalues (Floquet multipliers) of any infinite amplitude fixed points (limit cycles) in the imperfect system are identical to those of the corresponding solution of the associated spherical system for the perfect problem already computed, i.e.,  $s_2^{u_\infty} = s_2^u$ ,  $s_3^{u_\infty} = s_3^u$ , etc. Eqs. (3) and (13) show that the radial eigenvalue of an infinite amplitude fixed point in terms of the  $\rho$  variable is the negative of the radial eigenvalue of the corresponding finite amplitude fixed point in terms of the  $r$  variable. Thus, if a finite amplitude fixed point in the perfect system is radially unstable the corresponding infinite amplitude fixed point in the imperfect system is radially stable, and vice versa; a similar statement holds for the  $qp$  solutions. In particular, if a solution branch is subcritical in the perfect system there is a corresponding infinite amplitude solution of the imperfect system which is radially stable for  $\lambda > 0$ . In our scenario, a burst occurs for  $\lambda > 0$  when a trajectory follows the stable manifold of a fixed point (or a limit cycle)  $B \in \Sigma$  that is *unstable* within  $\Sigma$ . The instability within  $\Sigma$  then kicks the trajectory towards another fixed point (or limit cycle)  $A \in \Sigma$ . If this point has an unstable  $\rho$  eigenvalue the trajectory escapes from  $\Sigma$  towards finite amplitudes, forming a burst. If  $\Delta\lambda$  and/or  $\Delta\omega \neq 0$  a value of  $\lambda$  may be found for which the unstable manifold of  $A$  lies within the stable manifold of  $B$  forming a heteroclinic cycle  $B \rightarrow A \rightarrow B$ . The bursts then repeat. We now classify all cycles of this type.

#### 4.2. Codimension one heteroclinic cycles involving infinite amplitude solutions

Bursting behavior occurs for parameter values near those for which a heteroclinic cycle exists between infinite amplitude solutions. To specify a heteroclinic cycle we identify symmetry-related solutions (technically, we identify solutions with conjugate isotropy subgroups, i.e., solutions on the same group orbit [18]). Such a cycle between two infinite amplitude ( $\rho = 0$ ) solutions  $A$  and  $B$  will exist if the following conditions hold:

- (i)  $A$  is supercritical and  $B$  is subcritical for the perfect problem.
- (ii) There is a trajectory  $B \rightarrow A$  in the  $\Sigma$  subspace; this is possible if, within this subspace, or equivalently, for the perfect problem within the associated spherical system,
  - $B = \text{source}$  and  $A = \text{sink}$ ,
  - $B = \text{source}$  and  $A = \text{saddle}$ ,
  - $B = \text{saddle}$  and  $A = \text{sink}$ , or
  - $B = \text{saddle}$  and  $A = \text{saddle}$ .

Table 3 lists possible candidates for  $A$  and  $B$  when  $-3 < B_R < -1$ ,  $C_R = -1$ . The connecting trajectories are structurally stable to changes in  $\lambda$  because the dynamics in the  $\rho = 0$  subspace are independent of  $\lambda$ .

- (iii) There is a trajectory  $A \rightarrow B$  out of the  $\Sigma$  subspace which exists for some value of the bifurcation parameter  $\lambda$ . The existence of such a trajectory must be demonstrated numerically.

Since the existence of the resulting heteroclinic cycle depends only on the parameter  $\lambda$ , it is a codimension one phenomenon. To enumerate all situations for which a heteroclinic cycle of this type may exist, we restrict attention to the parameter range  $-3 < B_R < -1$ ,  $C_R = -1$ . For this parameter range, periodic orbits and heteroclinic orbits in the associated spherical system are considered to be sinks (see Tables 3 and 4) and we deduce that the only

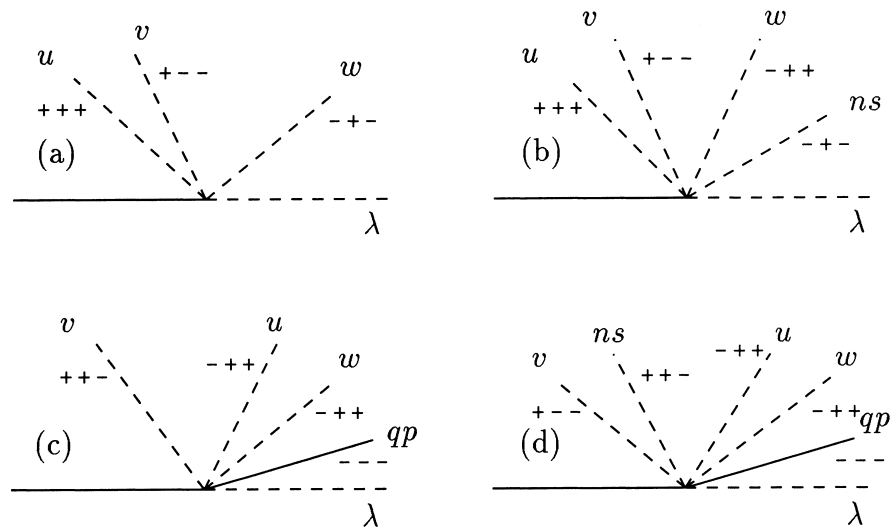


Fig. 2. All bifurcation diagrams for the perfect system with the connections  $B \rightarrow A$  of the type required for the existence of heteroclinic cycles involving infinite amplitude solutions when  $-3 < B_R < -1$ ,  $C_R = -1$  and  $B_I$  and  $C_I$  are chosen to be in (a) region  $IV_w$  ( $A = w$ ,  $B = u$ ), (b) region III ( $A = ns$ ,  $B = u$ ), (c) region I ( $A = qp$ ,  $B = v$ ), (d) region II ( $A = qp$ ,  $B = ns$ ). Solid (dashed) lines indicate stable (unstable) solution branches. The signs of the eigenvalues are indicated by + and -, with the first indicating radial stability. Parameter symmetries allow one to find possible heteroclinic connections involving other types of infinite amplitude solutions. For the heteroclinic cycle to exist there must also be a trajectory from  $A \rightarrow B$  out of the  $\Sigma$  subspace. The branch names are defined in Section 3.

possible ways to satisfy conditions (i) and (ii) are those shown in Fig. 2. By using parameter symmetries we can find possible heteroclinic cycles between other types of infinite amplitude solutions. In particular since these symmetries can change the  $qp$  solution from a libration present in the above parameter range to a rotation in other regimes the parameter symmetries can be used to generate necessary conditions for heteroclinic cycles involving rotations. However, since the trajectory from  $A \rightarrow B$  out of the  $\Sigma$  subspace described in condition (iii) is not necessarily preserved under the action of a parameter symmetry its presence must be demonstrated numerically for each set of parameters. Note that no cycles involving the heteroclinic orbit separating librations and rotations in the associated spherical system are possible.

We now briefly describe some manifestations of the presence of heteroclinic cycles involving infinite amplitude solutions in the bifurcation diagrams; these are illustrated in the examples which follow. The heteroclinic cycles may be analyzed within the three-dimensional system (3)–(5). First, suppose that  $A$  and  $B$  are infinite amplitude ( $\rho = 0$ ) fixed points in this system. If  $A$  ( $B$ ) has complex (real) eigenvalues in  $\Sigma$ , a Shil'nikov-like analysis [19,20] is possible. The analysis shows that a periodic solution branch may undergo an infinite number of saddle-node bifurcations  $\{\lambda_n\}$  as the branch is followed to higher period, with  $\lambda_{2j} \rightarrow \lambda_c+$  and  $\lambda_{2j+1} \rightarrow \lambda_c-$  as  $j \rightarrow \infty$ . Here  $\lambda_c$  is the parameter value at which the heteroclinic cycle forms. If  $A$  is an infinite amplitude limit cycle (i.e.,  $A = qp_\infty$ ) and  $B$  is an infinite amplitude fixed point, an analysis along the lines of [21] becomes possible provided parameters (such as  $C_R$ ) are chosen so that  $A$  has just undergone a Hopf bifurcation. In the present problem, the unstable (stable) manifold of  $A$  ( $B$ ) is a tubular (planar) two-dimensional surface out of  $\Sigma$ ; we denote these manifolds by  $W^U(A)$  ( $W^S(B)$ ). Suppose that for a particular  $\lambda$  (say  $\lambda_{c1}$ )  $W^U(A)$  becomes tangent to  $W^S(B)$ . In the presence of a (structurally stable) trajectory  $B \rightarrow A$  within  $\Sigma$  (see (ii) above) this tangency implies the formation of a heteroclinic cycle at  $\lambda_{c1}$ . For slightly larger  $\lambda$  the tube  $W^U(A)$  will intersect  $W^S(B)$  along two distinct lines corresponding to the presence of two distinct heteroclinic cycles at the same  $\lambda$  value. These cycles are structurally

stable, but unlike the situation studied in [18] this does not depend on the presence of fixed-point subspaces of  $A$  and  $B$ . Finally, when  $\lambda$  is increased far enough the tube  $W^U(A)$  emerges on the other side of  $W^S(B)$ , forming a last tangency at, say,  $\lambda = \lambda_{c2} > \lambda_{c1}$ . Analysis of this process implies, cf. [21], that periodic solutions may undergo an infinite number of saddle-node bifurcations at  $\lambda = \{\lambda_n\}$  as the branch is followed to higher period, with the sequences  $\{\lambda_{2j}\}$  and  $\{\lambda_{2j+1}\}$  tending to the two *different* values  $\lambda_{c1}$  and  $\lambda_{c2}$  as  $j \rightarrow \infty$  (see, in particular, Fig. 5 of [21]). As the Hopf bifurcation of  $A$  is approached (by varying  $C_R$ ) these two heteroclinic cycles “merge” (the tubular  $W^U(A)$  shrinks to a line) and beyond the Hopf bifurcation only a single heteroclinic cycle exists (at  $\lambda = \lambda_c$ ) connecting the resulting infinite amplitude fixed points.

We call such infinite sequences of saddle-node bifurcations along a periodic solution branch “Shil’nikov-like behavior” and describe several examples in Section 4.3. In addition, near each saddle-node bifurcation there is a period-doubling bifurcation [22], or if the periodic orbit is reflection-symmetric a symmetry-breaking pitchfork bifurcation [23]. The branch of periodic solutions that results may itself form a subsidiary heteroclinic cycle when followed to higher period, or it may reconnect to the same branch at another period-doubling or symmetry-breaking pitchfork bifurcation, forming a bifurcation “bubble” [24].

For branches which form heteroclinic cycles involving infinite amplitude solutions when followed to higher period, we find numerically that the average value of  $r$ ,  $\langle r \rangle$ , may locally increase or decrease, but  $\langle r \rangle$  is larger at the saddle-node bifurcation at  $\lambda_{k+2}$  than at  $\lambda_k$ ; in the resulting bifurcation diagrams  $\langle r \rangle$  versus  $\lambda$  the branch “spirals off to infinity.” Sometimes, however, the oscillatory branch collides with a branch of finite amplitude fixed points; if this finite amplitude fixed point has complex eigenvalues the resulting heteroclinic cycle may also give rise to Shil’nikov-like behavior, while if it has real eigenvalues homoclinic explosions may be encountered [25]. When such a global bifurcation is approached the periodic orbit on the branch spends more and more time near the fixed point(s) and  $\langle r \rangle$  approaches the value of  $r$  for these fixed point(s). This is in contrast to heteroclinic cycles involving infinite amplitude solutions for which the trajectory reaches and returns from infinity in finite time  $t$  (see Appendix C); such heteroclinic cycles thus describe bursts of *finite* duration.

Finally, because symmetry-related solutions may have different physical manifestations it is also useful to consider the heteroclinic *network*, defined to be the set of all heteroclinic connections associated with a heteroclinic cycle in which symmetry-related solutions are *not* identified. This concept is important because on reaching an infinite amplitude state  $B$  that is a saddle in  $\Sigma$  a trajectory can exit in one of two directions which take it to different but symmetry-related states  $A$  and  $A'$ . Some consequences of the presence of networks will be explored in the examples below.

#### 4.3. Numerical studies of the imperfect system

Following [12] we focus on parameter values for which the perfect system has subcritical  $u$  solutions and supercritical  $v$ ,  $w$  solutions. The coefficients  $B$  and  $C$  will be used to control whether the  $ns$  and/or  $qp$  solutions are also present. We use the *dstool* [26] simulation package to solve the differential equations with a fourth-order, variable-step Runge–Kutta integration scheme, and AUTO [27] to follow solution branches and detect bifurcations. For different purposes different variables are useful. For example, it is often easiest numerically to work in the  $(\rho, \theta, \phi)$  coordinates because this makes the large  $r$  behavior associated with bursts more manageable. The eigenvalues reported in this section are all calculated using Eqs. (13)–(15). However, the variables  $(u, v, w)$  highlight the symmetry properties of the solutions and are therefore used in many of the phase space plots. Time series showing the bursting behavior will be plotted as  $r = |z_+|^2 + |z_-|^2 = \sqrt{u^2 + v^2 + w^2} = 1/\rho$  versus  $t$ . Bursts are associated with small  $\rho$  values, or equivalently, with large excursions from the neighborhood of  $(u, v, w) = (0, 0, 0)$ . In the phase space plots plus signs, squares, and diamonds indicate saddles, sources, and sinks, respectively.

The bifurcation diagrams typically show

$$\langle r \rangle \equiv \frac{1}{T} \int_0^T r dt = \frac{T_\tau}{\int_0^{T_\tau} \rho d\tau} \quad (16)$$

as a function of the bifurcation parameter  $\lambda$ . Here  $T$  is the period of the solution in the original time  $t$ , and  $T_\tau$  is the period of the solution to Eqs. (13)–(15) found in terms of the rescaled time  $\tau$ . Since the bursts are fast events in the time  $t$  (see Appendix C), the average  $\langle r \rangle$  for a sequence of large amplitude bursts may in fact be quite small. However, for heteroclinic cycles involving infinite amplitude solutions Eq. (16) shows that  $\langle r \rangle = \infty$ . The presence of such heteroclinic cycles can have a dramatic effect as discussed in the examples that follow. In the bifurcation diagrams solid (broken) lines indicate stable (unstable) solutions; circles, diamonds, squares, and triangles indicate Hopf, saddle-node, period-doubling, and symmetry-breaking pitchfork bifurcations, respectively. Many period-doubled branches are omitted. Often, saddle-node and period-doubling (or symmetry-breaking pitchfork) bifurcations occur at nearly the same value of  $\lambda$  due to rapid variation of one or more Floquet multipliers of the periodic solutions as the solution branch is followed. If the remaining nontrivial Floquet multiplier has modulus less than one between such a pair of bifurcations, there will be a small range of  $\lambda$  values in which the solutions are stable. Moreover, branches which arise from period-doubling (or symmetry-breaking pitchfork) bifurcations often undergo period-doubling bifurcations themselves near the  $\lambda$  values at which they come into existence; if the other nontrivial Floquet multiplier has modulus less than one between the subsequent period-doubling bifurcations, there will be a small range of  $\lambda$  values in which period-two solutions are stable. In the following we use RS (NRS) to indicate that a periodic or chaotic solution to the three-dimensional system is symmetric (not symmetric) with respect to the symmetry  $\kappa_1$ . For a RS periodic orbit, the action of  $\kappa_1$  is equivalent to time translation by half a period. The symmetries of chaotic solutions may be thought of as symmetries *on average*.

We now examine a number of examples chosen to illustrate different types of dynamical behavior. The eigenvalues and Floquet multipliers of the infinite amplitude solutions involved in heteroclinic cycles in the examples that follow are summarized in Table 5.

#### 4.3.1. Example 1(a)

When

$$A = 1 - 1.5i, \quad B = -2.8 + 5i, \quad C = 1 + i; \quad \Delta\lambda = \Delta\omega = 0,$$

the  $u$  solutions are subcritical, the  $v$ ,  $w$ , and  $qp$  solutions are supercritical, and the  $ns$  solutions are absent. Application of the parameter symmetry  $P_2$  brings these parameters into the range  $-3 < B_R < -1$ ,  $C_R = -1$  and region I of parameter space; this corresponds to case (c) of Fig. 2, suggesting the possibility of a heteroclinic cycle involving infinite amplitude solutions. In the original parameters this translates to the possibility of a heteroclinic cycle involving the  $u_\infty$  (saddle within  $\Sigma$ ) and  $qp_\infty$  (sink within  $\Sigma$ ) solutions. The (partial) bifurcation diagram for  $\Delta\lambda = 0.03$ ,  $\Delta\omega = 0.02$  is compared with the bifurcation diagram for  $\Delta\lambda = \Delta\omega = 0$  in Fig. 3. As  $|\lambda|$  becomes large, the behavior of the imperfect system approaches the behavior of the perfect system. In particular, the  $w_e$  and  $w_o$  branches given by Eqs. (11) and (12) approach the  $w$  branch for the perfect problem. In addition to the two primary bifurcations responsible for the  $w_{e,o}$  branches the bifurcation diagram reveals the presence of a *disconnected* branch of fixed points. This branch, labeled  $u/v$ , must be computed numerically; as  $\lambda \rightarrow -\infty$  ( $+\infty$ ) the fixed points on this branch approach the  $u$  ( $v$ ) fixed points for the perfect system (hence the name). Finally, the Hopf bifurcation at  $\lambda = 0.180681$  gives rise to a stable periodic orbit which approaches the stable  $qp$  solution for the perfect problem as  $\lambda \rightarrow \infty$ .

Table 5  
Eigenvalues and Floquet multipliers from Eqs. (13)–(15) for the infinite amplitude solutions involved in heteroclinic cycles for the examples of Section 4.3. The eigenvalues and Floquet multipliers with subscripts 1 (2,3) correspond to perturbations out of (within) the  $\Sigma$  subspace. All are independent of  $\lambda$  and hence are identical for all heteroclinic cycles that exist.

Example	$B$	$A$
1(a)	$u_\infty$ $s_1^{u_\infty} = -0.200$ $s_2^{u_\infty} = -5.868$ $s_3^{u_\infty} = 0.0682$	$qp_\infty$ $FM_1=57.46$ $FM_2=1.000$ $FM_3=0.604$
1(b)	$u_\infty$ $s_1^{u_\infty} = -0.150$ $s_2^{u_\infty} = -5.801$ $s_3^{u_\infty} = 0.151$	$qp_\infty$ $FM_1=45.19$ $FM_2=1.000$ $FM_3=0.894$
2	$u_\infty$ $s_1^{u_\infty} = -0.100$ $s_2^{u_\infty} = -5.734$ $s_3^{u_\infty} = 0.234$	$v_\infty$ $s_1^{v_\infty} = 1.700$ $s_2^{v_\infty} = -0.05 + 2.929i$ $s_3^{v_\infty} = -0.05 - 2.929i$
3	$ns_\infty$ $s_1^{ns_\infty} = -0.164$ $s_2^{ns_\infty} = -5.723$ $s_3^{ns_\infty} = 0.0319$	$qp_\infty$ $FM_1=77.97$ $FM_2=1.000$ $FM_3=0.581$
4	$ns_\infty$ $s_1^{ns_\infty} = -0.0322$ $s_2^{ns_\infty} = -5.384$ $s_3^{ns_\infty} = 0.0870$	$v_\infty$ $s_1^{v_\infty} = 1.730$ $s_2^{v_\infty} = -0.005 + 2.598i$ $s_3^{v_\infty} = -0.005 - 2.598i$

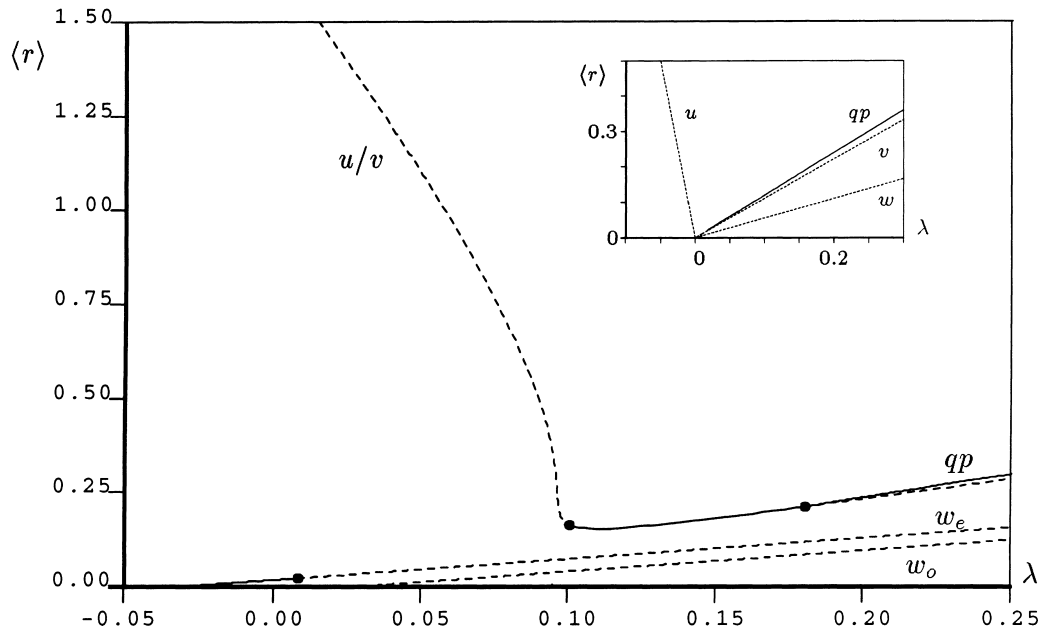


Fig. 3. Partial bifurcation diagram for  $A = 1 - 1.5i, B = -2.8 + 5i, C = 1 + i$  and  $\Delta\lambda = 0.03, \Delta\omega = 0.02$ . The Hopf bifurcations on the  $w_e$  branch at  $\lambda = 0.00857143$  and on the  $u/v$  branch at  $\lambda = 0.100750$  are indicated but the resulting branches are omitted (see Fig. 4). In contrast to the perfect system (inset) with a stable  $qp$  primary branch, the stable primary branch in the imperfect system is the  $w_e$  branch.

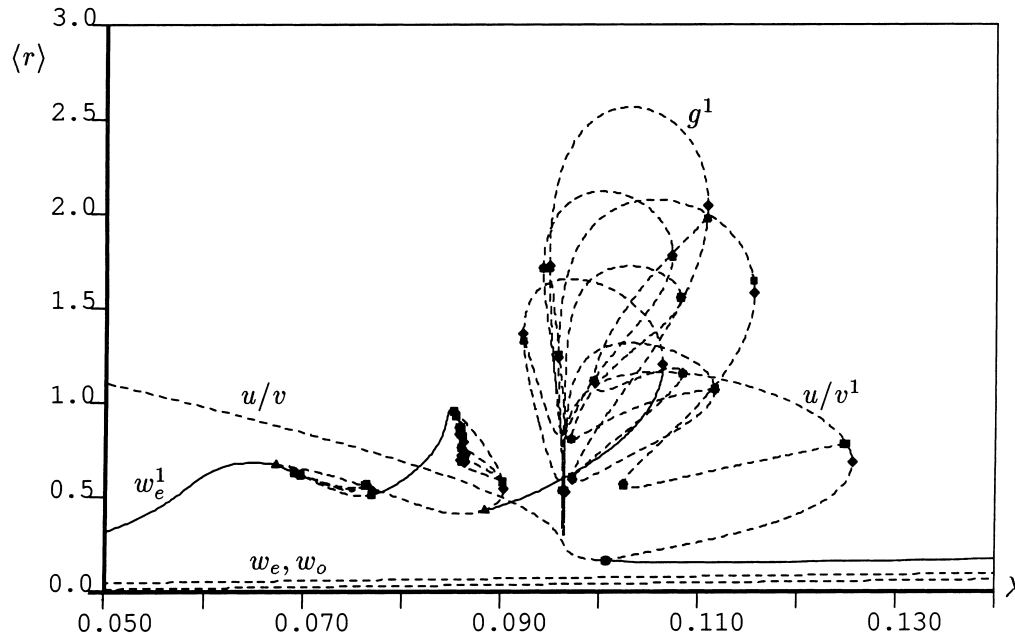


Fig. 4. Detailed bifurcation diagram for the parameters  $A = 1 - 1.5i$ ,  $B = -2.8 + 5i$ ,  $C = 1 + i$ , and  $\Delta\lambda = 0.03$ ,  $\Delta\omega = 0.02$ . Not all period-doubled branches are shown.

Fig. 4 shows the results of a detailed bifurcation study for these parameters [12]; however, not all period-doubled branches are shown. The  $w_e^1$  branch arises from the Hopf bifurcation on the  $w_e$  branch at  $\lambda = 0.00857143$ ; each trajectory on this branch visits the vicinity of different (but symmetry-related)  $u_\infty$  fixed points. These solutions are rotations. The  $u/v^1$  branch is born in a Hopf bifurcation on the  $u/v$  branch at  $\lambda = 0.100750$ ; each trajectory along this branch visits repeatedly the vicinity of *same* infinite amplitude fixed point. These solutions are librations. The  $g^1$  branch will be described later. Notice that the  $w_e^1$  solutions are stable for large ranges of  $\lambda$  values (for example, for  $0.0885 < \lambda < 0.1065$ ) while the  $u/v^1$  solutions are stable for much smaller ranges (for example, for  $0.1250 < \lambda < 0.1256$ ). In fact, for this range the stable  $u/v^1$  solutions coexist with stable  $u/v$  solutions which are more likely to be observed if  $\lambda$  is ramped upwards from below 0.1250. We now describe the major characteristics of this bifurcation diagram.

(a) *Heteroclinic cycle involving infinite amplitude solutions.* As argued above, this example offers the possibility of a heteroclinic cycle involving the  $u_\infty$  and  $qp_\infty$  solutions. Examples of such cycles are shown in Fig. 5. Here the effect of these cycles is local; the branches which might be expected to be affected by the heteroclinic cycles (e.g., the  $w_e^1$  and  $u/v^1$  branches) in fact terminate in global bifurcations involving finite amplitude  $u/v$  fixed points, i.e., instead of undergoing an infinite number of saddle-node bifurcations as they are followed to higher period, these branches only undergo a *finite* number before colliding with the finite amplitude  $u/v$  fixed points.

(b) *Global bifurcations involving finite amplitude fixed points.* The  $u/v$  fixed points do not lie in the reflection-invariant subspace  $\text{Fix}(\langle\kappa_1\rangle) \equiv \{(u, v, w) | u = v = 0\}$ ; thus there are two  $u/v$  solutions related by  $\kappa_1$ . Consequently, RS *heteroclinic* orbits connecting the two  $\kappa_1$ -related  $u/v$  fixed points or two  $\kappa_1$ -related *homoclinic* orbits to the  $\kappa_1$ -related  $u/v$  fixed points are both possible. The existence of these orbits is suggested by following many solution branches (e.g., the  $w_e^1$  and  $u/v^1$  branches) to very high period. As such a homoclinic or heteroclinic orbit is approached, the periodic orbit spends more and more time near the  $u/v$  fixed point(s) so that  $\langle r \rangle$  approaches the value of  $r$  for these fixed point(s) (see Fig. 6).

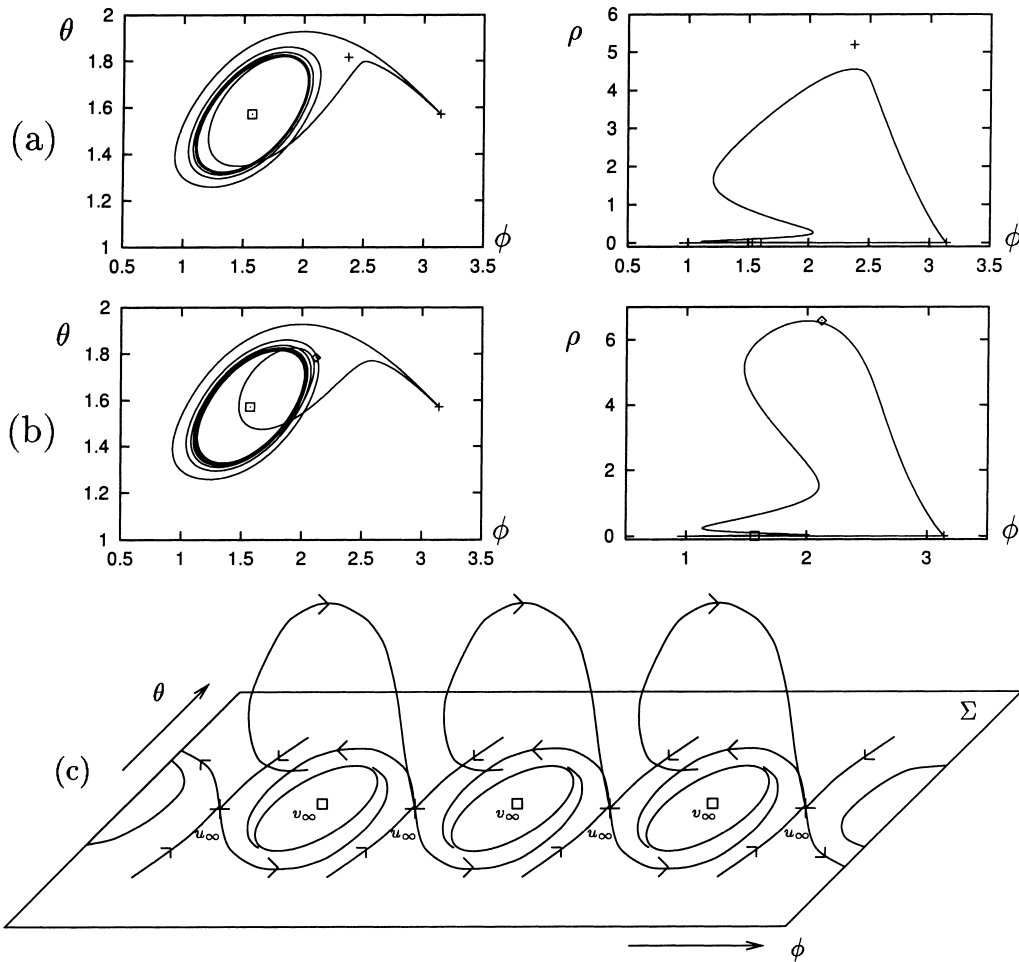


Fig. 5. (a) A numerically calculated heteroclinic cycle involving the infinite amplitude fixed point  $u_\infty$  and the infinite amplitude limit cycle  $qp_\infty$  at  $\lambda = 0.0974$ . (b) Another heteroclinic cycle exists at  $\lambda = 0.110$ . (c) Sketch of the resulting complete heteroclinic network showing all connections.

Fig. 7 shows a *heteroclinic* orbit for  $\lambda = 0.0964187$  connecting two  $u/v$  fixed points related by  $\kappa_1$ ; another such orbit exists for  $\lambda = 0.09654768$ . At these global bifurcations the  $u/v$  fixed points have purely real eigenvalues  $s_1 > s_2 > 0 > s_3$  (see Fig. 8); since  $|s_2/s_3| < 1$  we expect that the global bifurcations will lead to homoclinic explosions as for the Lorenz equations (but with time reversed from the case which is typically studied) [20,25]. We have located a solution branch which is born in one of these global bifurcations and terminates in the other. An example of a stable solution on this branch (which we call a  $g^1$  solution; such a solution is RS) and a bifurcation diagram is shown in Fig. 9. Finally, Fig. 10 shows two  $\kappa_1$ -related *homoclinic* orbits which exist for  $\lambda = 0.0962724$ ; similar orbits exist also for  $\lambda = 0.0964974$ . Because there is only one homoclinic orbit for each fixed point, these global bifurcations do not produce homoclinic explosions [20].

(c) *Complicated behavior for  $0.065 < \lambda < 0.092$ .* The range  $0.065 < \lambda < 0.092$  contains much complicated behavior including period-doubling cascades to strange attractors, periodic windows, and symmetry-increasing bifurcations of strange attractors [28]. These are conveniently described using (approximately one-dimensional) Poincaré maps which take into account the reflection symmetry. We let

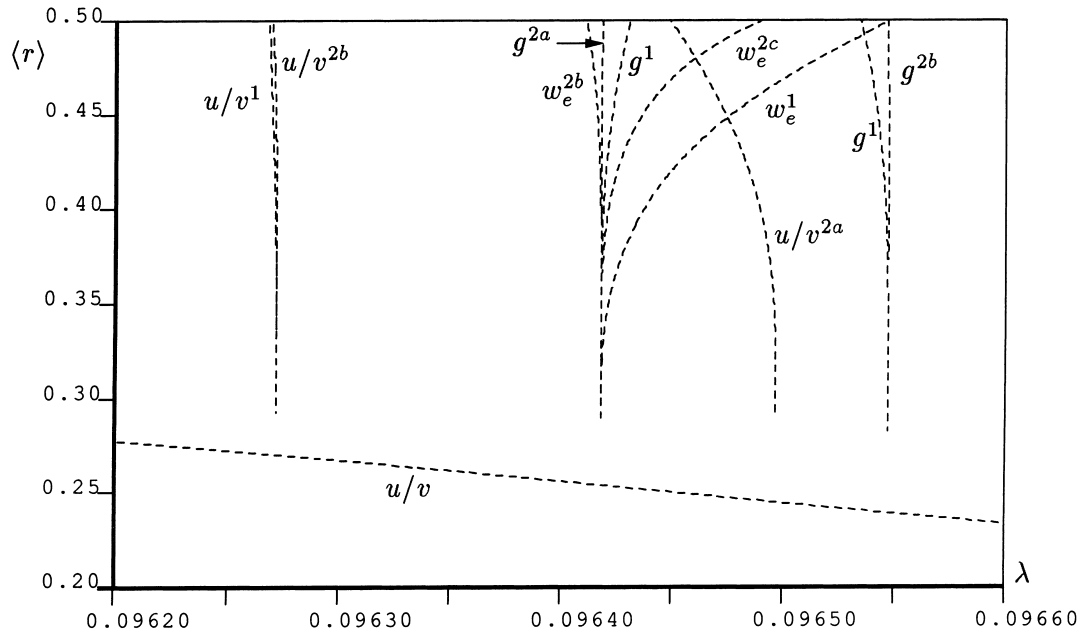


Fig. 6. Bifurcation diagram showing global bifurcations involving the finite amplitude  $u/v$  fixed points. The  $u/v^{2a}$  and  $u/v^{2b}$  branches arise from period-doubling bifurcations from the  $u/v^1$  branch, while the  $w_e^{2b}$ ,  $w_e^{2c}$ ,  $g^{2a}$ , and  $g^{2b}$  branches arise from symmetry-breaking pitchfork bifurcations from the  $w_e^1$  and  $g^1$  branches.

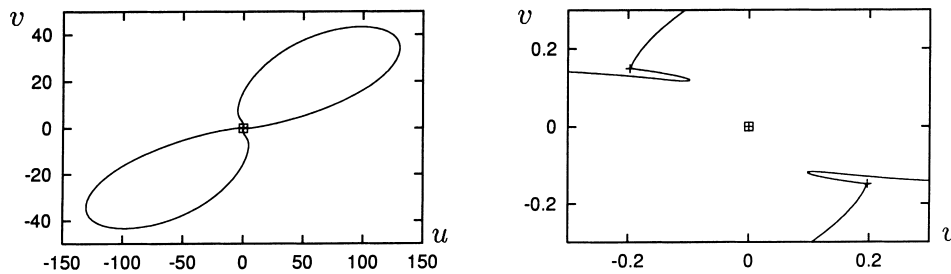


Fig. 7. The RS heteroclinic orbit connecting two  $\kappa_1$ -related  $u/v$  fixed points at  $\lambda = 0.0964187$  with  $r_{\max} \approx 166$ . The frame at right shows a blow-up of the frame at left. Another RS heteroclinic orbit exists at  $\lambda = 0.09654768$  with  $r_{\max} \approx 7378$ . Here  $r_{\max}$  denotes the maximum value of  $r$  along the orbit.

$$\Sigma_+ = \{(u, v, w) | u = v, u > 0\},$$

$$\Sigma_- = \{(u, v, w) | u = v, u < 0\},$$

and define the Poincaré maps  $P : \Sigma_+ \rightarrow \Sigma_+$ ,  $\tilde{P} : \Sigma_+ \rightarrow \Sigma_-$ . All periodic orbits which pierce  $\Sigma_+$  are fixed points of  $P$ . Because of the  $\kappa_1$  symmetry the map from  $\Sigma_-$  to  $\Sigma_+$  is identical to  $\tilde{P}$  so that  $P = \tilde{P} \cdot \tilde{P}$ . For a RS periodic orbit the action of  $\tilde{P}$  is the same as the action of  $\kappa_1$ ; thus RS periodic orbits are fixed points of  $\kappa_1 \cdot \tilde{P}$  in addition to being fixed points of  $P$ . On the other hand, NRS orbits are fixed points of  $P$  but not of  $\kappa_1 \cdot \tilde{P}$ . There may be RS and NRS periodic orbits embedded in a RS strange attractor; however, only NRS periodic orbits may be embedded in a NRS strange attractor, so for such attractors we expect that the map  $\kappa_1 \cdot \tilde{P}$  will not have any fixed points.

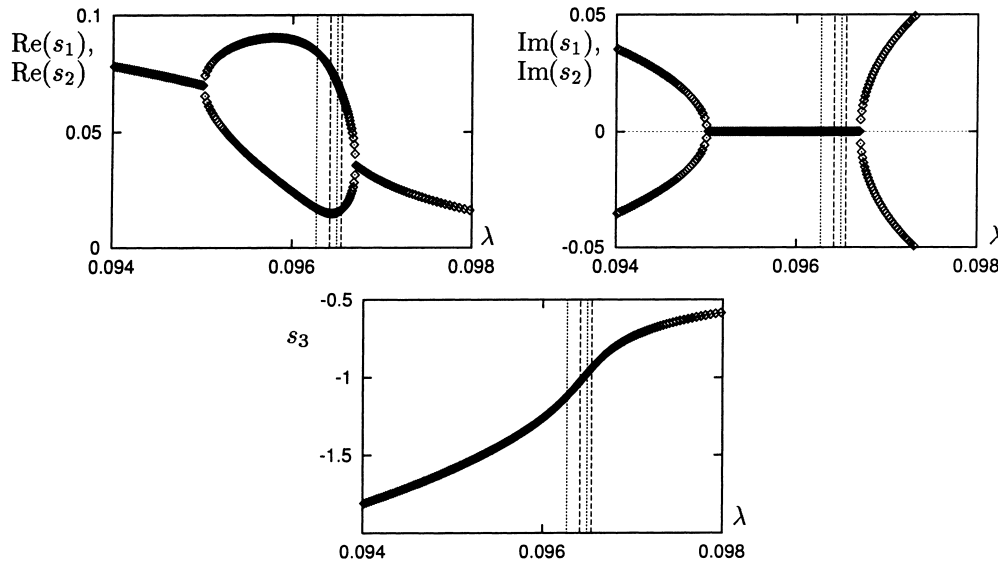


Fig. 8. Eigenvalues  $s_1, s_2$ , and  $s_3$  of the  $u/v$  fixed points; the former are real for  $0.0950 < \lambda < 0.0967$ . The vertical dashed (dotted) lines show the  $\lambda$  values for heteroclinic (homoclinic) bifurcations involving the finite amplitude  $u/v$  fixed points.

Fig. 11(a) shows a partial bifurcation diagram for  $0.065 < \lambda < 0.080$ . The RS  $w_e^1$  branch is born at a Hopf bifurcation on the  $w_e$  branch when  $\lambda = 0.00857143$ , and is stable until a symmetry-breaking pitchfork bifurcation at  $\lambda = 0.0672409$ . This bifurcation gives rise to two  $\kappa_1$ -related stable NRS periodic solutions which we call  $w_e^2$  solutions; for these solutions successive bursts differ in amplitude (see Fig. 12(a)). The  $w_e^2$  solutions undergo identical period-doubling cascades which accumulate at  $\lambda \approx 0.06975$  and lead to two  $\kappa_1$ -related NRS strange attractors. As  $\lambda$  is increased to 0.0701 a period 6 window (defined according to the number of successive bursts with distinct amplitudes) is formed with a periodic NRS orbit as shown in Fig. 12(b). As  $\lambda$  is increased further the period 6 orbit itself undergoes a period-doubling cascade so that by  $\lambda = 0.07013$  there are again two  $\kappa_1$ -related NRS strange attractors. At  $\lambda \approx 0.070319$  these strange attractors merge in a symmetry-increasing bifurcation as illustrated in Fig. 13. As  $\lambda$  is increased to 0.0707 a period 5 window is formed with a periodic RS orbit. This periodic orbit undergoes a symmetry-breaking pitchfork bifurcation and the resulting NRS periodic orbits then undergo period-doubling cascades leading to two  $\kappa_1$ -related NRS strange attractors. These attractors merge at  $\lambda \approx 0.070779$  giving a RS strange attractor. Similar behavior is found as  $\lambda$  is increased further, with other periodic windows (such as a period 7 window near  $\lambda = 0.07454$ ) which are destroyed in ways similar to those described above. There is a reverse period-doubling cascade which accumulates at  $\lambda \approx 0.0762$ . At  $\lambda = 0.0769685$  the  $w_e^2$  solutions regain stability.

The  $w_e^2$  solutions remain stable as  $\lambda$  is increased to 0.0852558 at which point they undergo a period-doubling bifurcation. In Fig. 11(b) we show the bifurcation diagram for  $0.085 < \lambda < 0.092$ . In this range there are again period-doubling cascades, periodic windows (including a period 3 window at  $\lambda = 0.088$ ), and symmetry-increasing bifurcations in which NRS strange attractors merge to form a RS strange attractor. A unique feature for this portion of the bifurcation diagram is the presence of many saddle-node and period-doubling bifurcations for  $0.0858 < \lambda < 0.0865$ ; the origin of this behavior has not been determined. At  $\lambda = 0.0884534$  the  $w_e^2$  branch reconnects with the  $w_e^1$  branch in a symmetry-restoring pitchfork bifurcation.

Complicated behavior such as that described here also occurs for appropriate  $\lambda$  values for the remaining examples, but will not be emphasized.

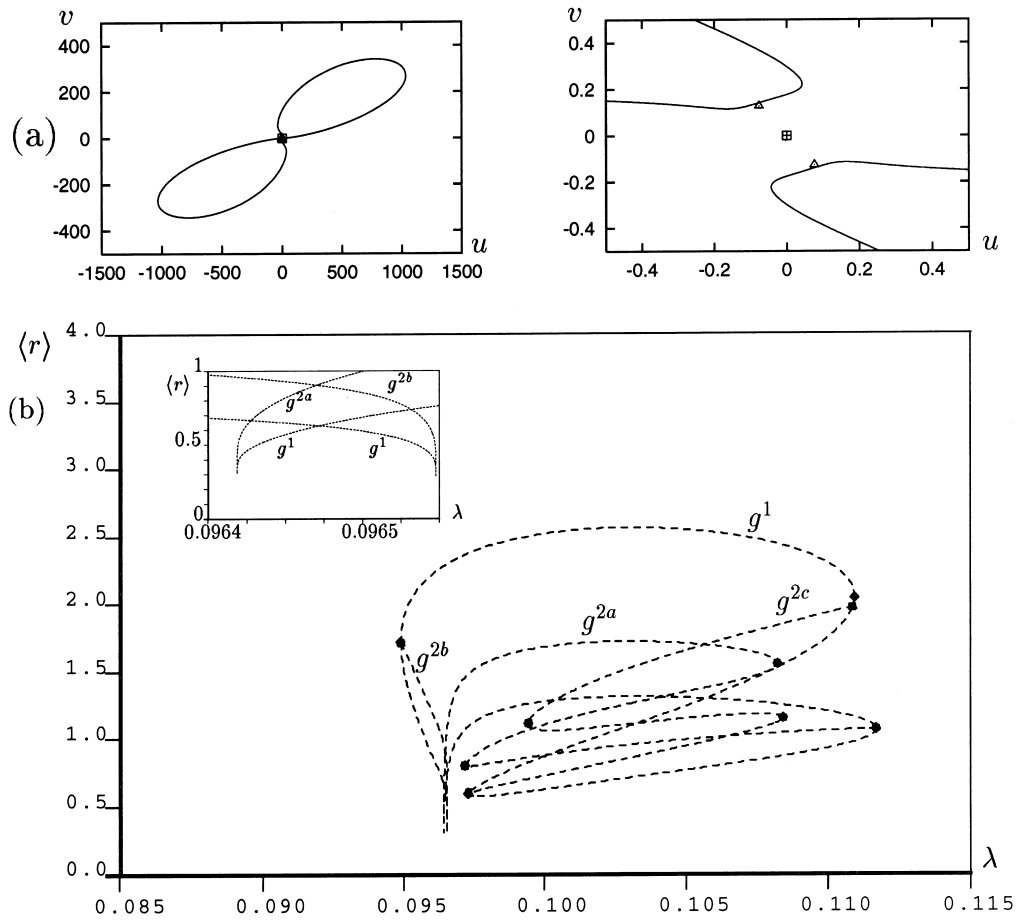


Fig. 9. (a) Stable  $g^1$  solution for  $\lambda = 0.1109354$  with  $\langle r \rangle \approx 2.045$ . The frame at right shows a blow-up of the frame at left. (b) Bifurcation diagram showing the  $g^1$  branch and the branches which bifurcate off the  $g^1$  branch in symmetry-breaking pitchfork bifurcations. All subsequent period-doubled branches are omitted. Inset shows detail of (b).

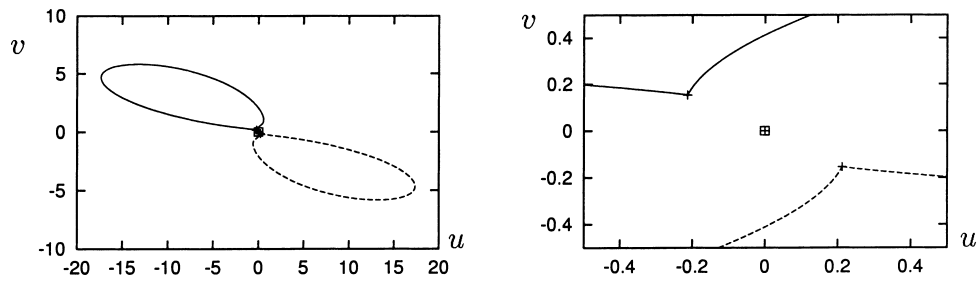


Fig. 10. The two  $\kappa_1$ -related homoclinic orbits to the  $\kappa_1$ -related  $u/v$  fixed points at  $\lambda = 0.0962724$  with  $r_{\max} \approx 18.2$ . The frame at right shows a blow-up of the frame at left. Such homoclinic orbits also exist at  $\lambda = 0.0964974$  with  $r_{\max} \approx 991$ .

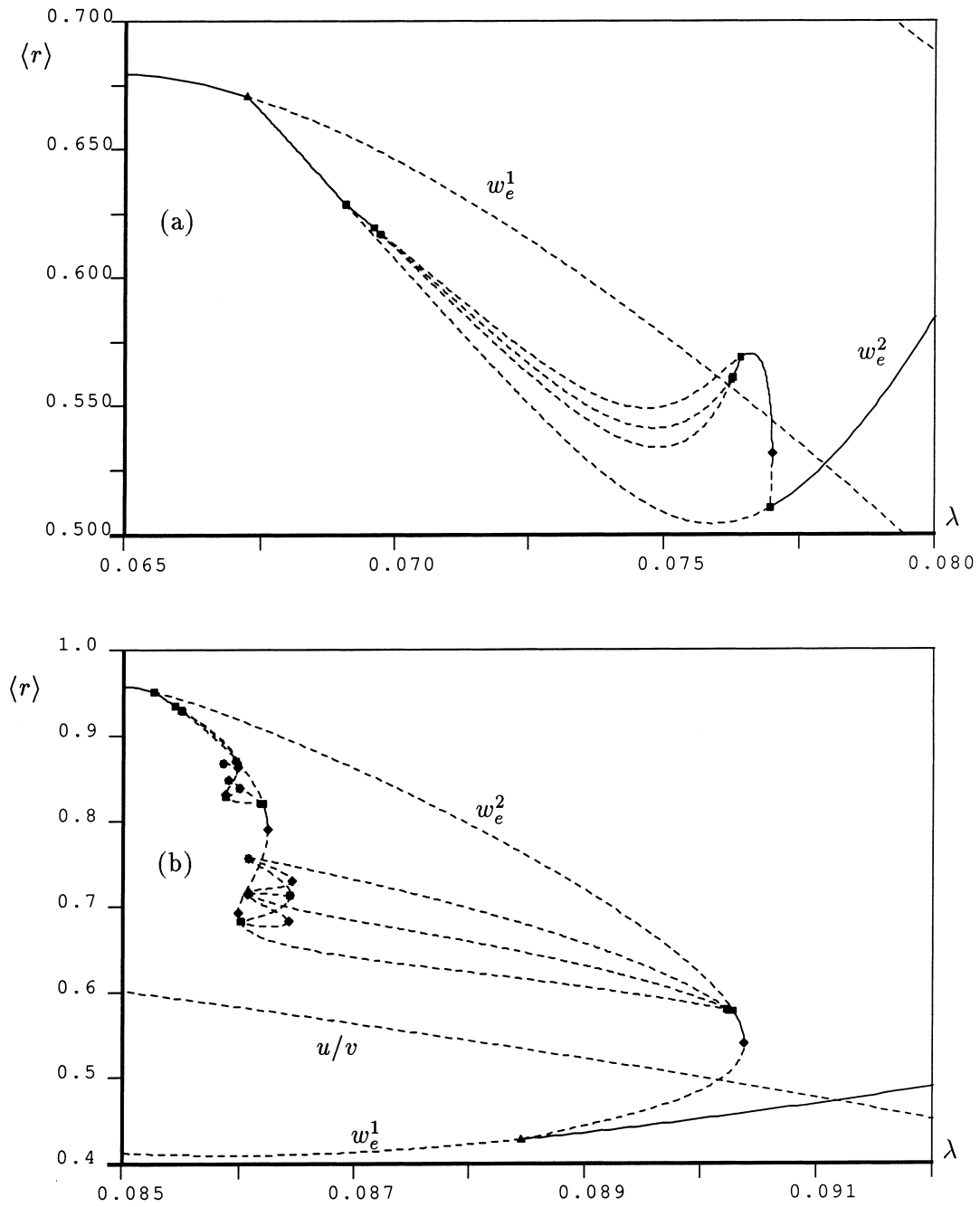


Fig. 11. Detail of the bifurcation diagram for (a)  $0.065 < \lambda < 0.080$  and (b)  $0.085 < \lambda < 0.092$ . Not all period-doubled branches are shown.

4.3.2. Example 1(b)

We now decrease the value of  $C_R$  choosing

$$A = 1 - 1.5i, \quad B = -2.8 + 5i, \quad C = 0.95 + i.$$

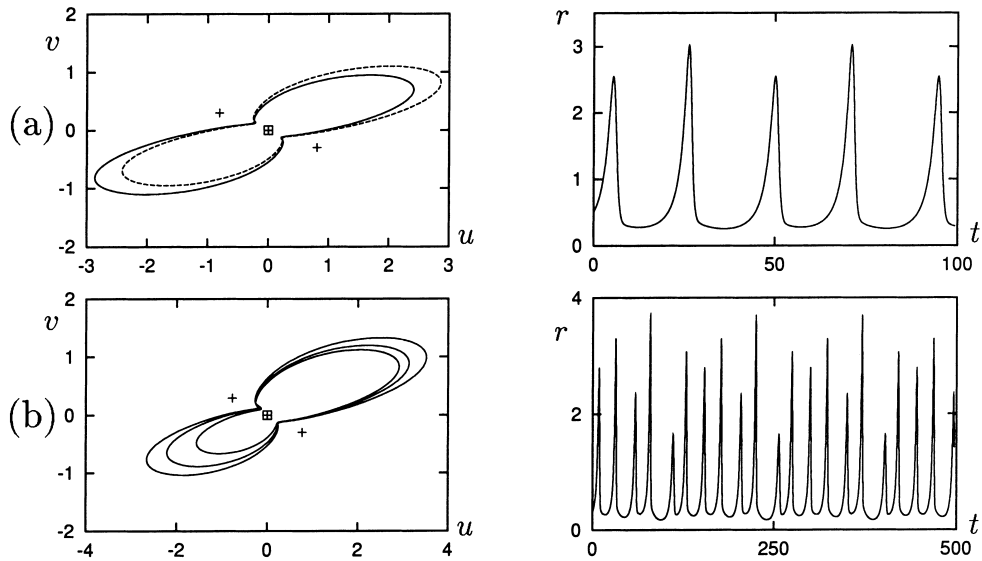


Fig. 12. (a) Two stable  $\kappa_1$ -related NRS  $w_c^2$  solutions at  $\lambda = 0.0675$  with  $\langle r \rangle \approx 0.665$ . At right is the time series for one of these solutions. (b) Stable NRS period 6 orbit and burst sequence at  $\lambda = 0.0701$ . The  $\kappa_1$ -related orbit is omitted.

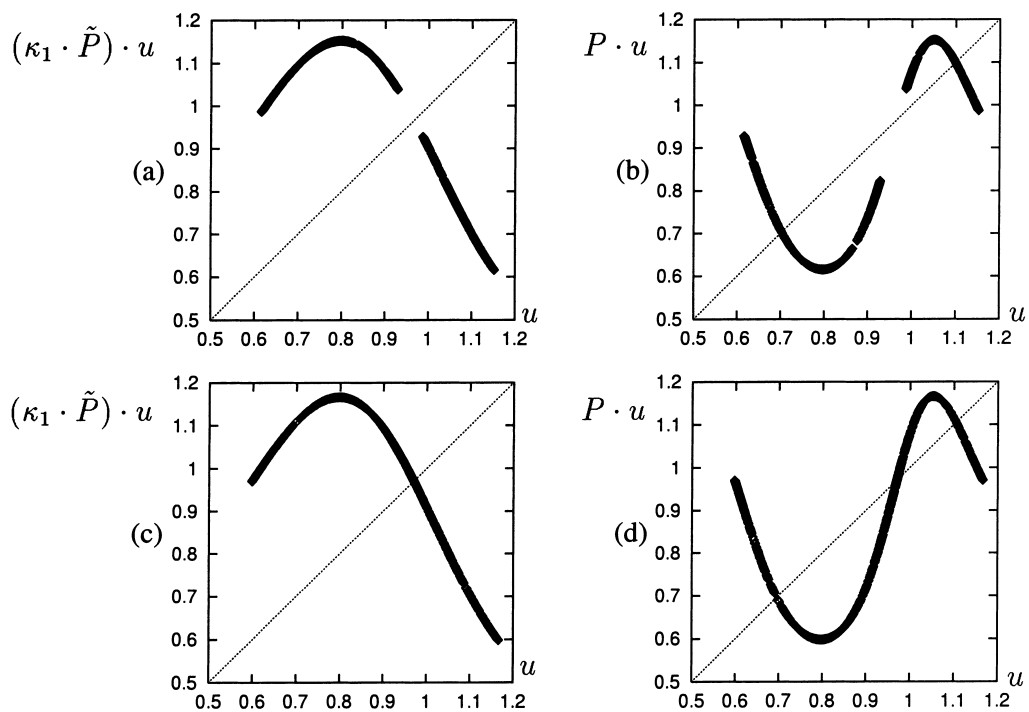


Fig. 13. The maps (a)  $\kappa_1 \cdot \tilde{P}$  and (b)  $P$  for the two  $\kappa_1$ -related NRS strange attractors when  $\lambda = 0.07013$ . The gap near  $(\kappa_1 \cdot \tilde{P}) \cdot u = u$  in (a) indicates that there are no RS periodic solutions embedded in these attractors. The two fixed points in (b) correspond to  $\kappa_1$ -related NRS periodic solutions. When  $\lambda$  is increased to 0.070319 a symmetry-increasing bifurcation occurs, and the  $\kappa_1 \cdot \tilde{P}$  map (c) has a fixed point indicating a RS periodic solution embedded in the strange attractor. The  $P$  map (d) has three fixed points, one corresponding to this RS periodic solution and the other two corresponding to  $\kappa_1$ -related NRS periodic solutions.

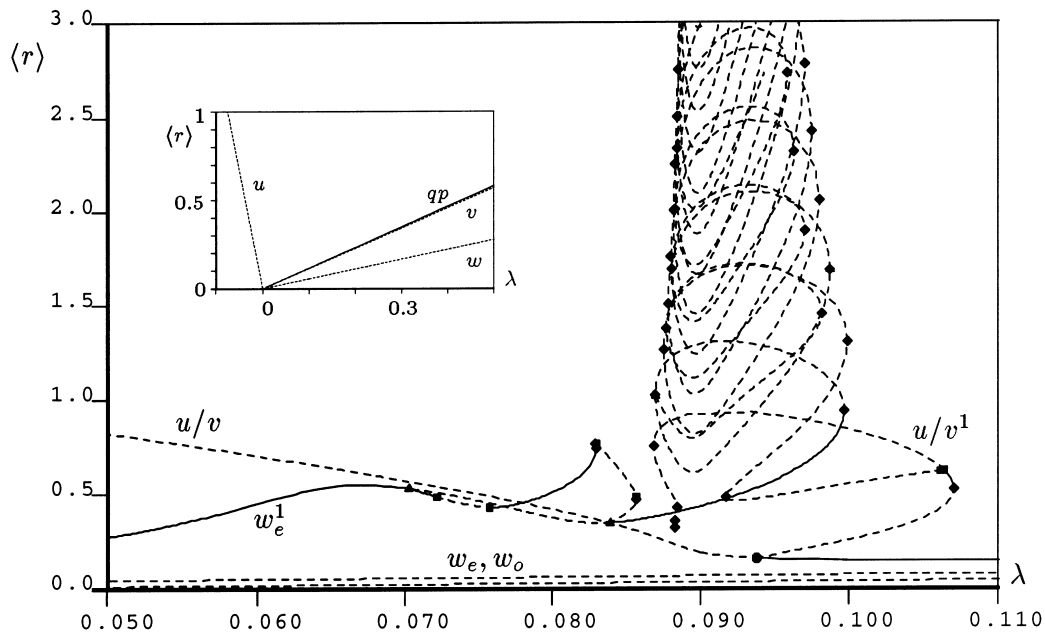


Fig. 14. Bifurcation diagram for the parameters  $A = 1 - 1.5i, B = -2.8 + 5i, C = 0.95 + i, \Delta\lambda = 0.03, \Delta\omega = 0.02$  for comparison with Fig. 4. Not all period-doubled branches are shown. The inset shows the corresponding bifurcation diagram for the perfect system.

When  $\Delta\lambda = \Delta\omega = 0$  the  $u$  solutions are still subcritical, the  $v, w$ , and  $qp$  solutions supercritical and the  $ns$  solutions absent. As before we take  $\Delta\lambda = 0.03, \Delta\omega = 0.02$ . Holding the other parameters fixed, the  $v_\infty$  solutions undergo a subcritical Hopf bifurcation which destroys the  $qp_\infty$  solutions as  $C_R$  decreases through  $-B_R/3 = 14/15 \approx 0.93333$ ; for the above parameter values the  $qp_\infty$  solution therefore still exists but the system is closer to a Hopf bifurcation. As in Example 1(a) application of the parameter symmetry  $P_2$  and rescaling of time brings these parameters into the range  $-3 < B_R < -1, C_R = -1$  and region I of parameter space, i.e., to case (c) of Fig. 2. The resulting bifurcation diagram is shown in Fig. 14, with branch names defined as in Example 1(a). The main point to be emphasized here is that although the  $u/v^1$  branch terminates in a global bifurcation involving the finite amplitude  $u/v$  fixed points as in Example 1(a), the  $w_e^1$  branch does not; instead, it undergoes Shil'nikov-like behavior due to a heteroclinic cycle involving the  $u_\infty$  and  $qp_\infty$  solutions. In this case the saddle-node bifurcations on the  $w_e^1$  solution branch accumulate, in the notation of Section 4.2, to  $\lambda_{c1} \approx 0.089$  and  $\lambda_{c2} \approx 0.095$ . Fig. 15 shows the period  $T_\tau/2$  between successive bursts on the  $w_e^1$  branch as a function of  $\lambda$  together with projections of the solution at two successive saddle-node bifurcations. As the period increases the number of turns near  $qp_\infty$  increases and the solutions become better and better approximations to heteroclinic cycles consisting of a trajectory connecting a  $u_\infty$  fixed point to a  $qp_\infty$  solution within  $\Sigma$ , followed by return trajectory lying outside  $\Sigma$  to another  $u_\infty$  fixed point shifted in  $\phi$  by  $\pi$  from the first one. Branches which arise from symmetry-breaking pitchfork and period-doubling bifurcations from the  $w_e^1$  and  $u/v^1$  branches, respectively, also show Shil'nikov-like behavior.

#### 4.3.3. Example 2

When  $C_R$  is decreased even further the  $qp_\infty$  solution is destroyed in a Hopf bifurcation on the  $v_\infty$  solution. Thus, when

$$A = 1 - 1.5i, \quad B = -2.8 + 5i, \quad C = 0.9 + i, \quad \Delta\lambda = \Delta\omega = 0,$$

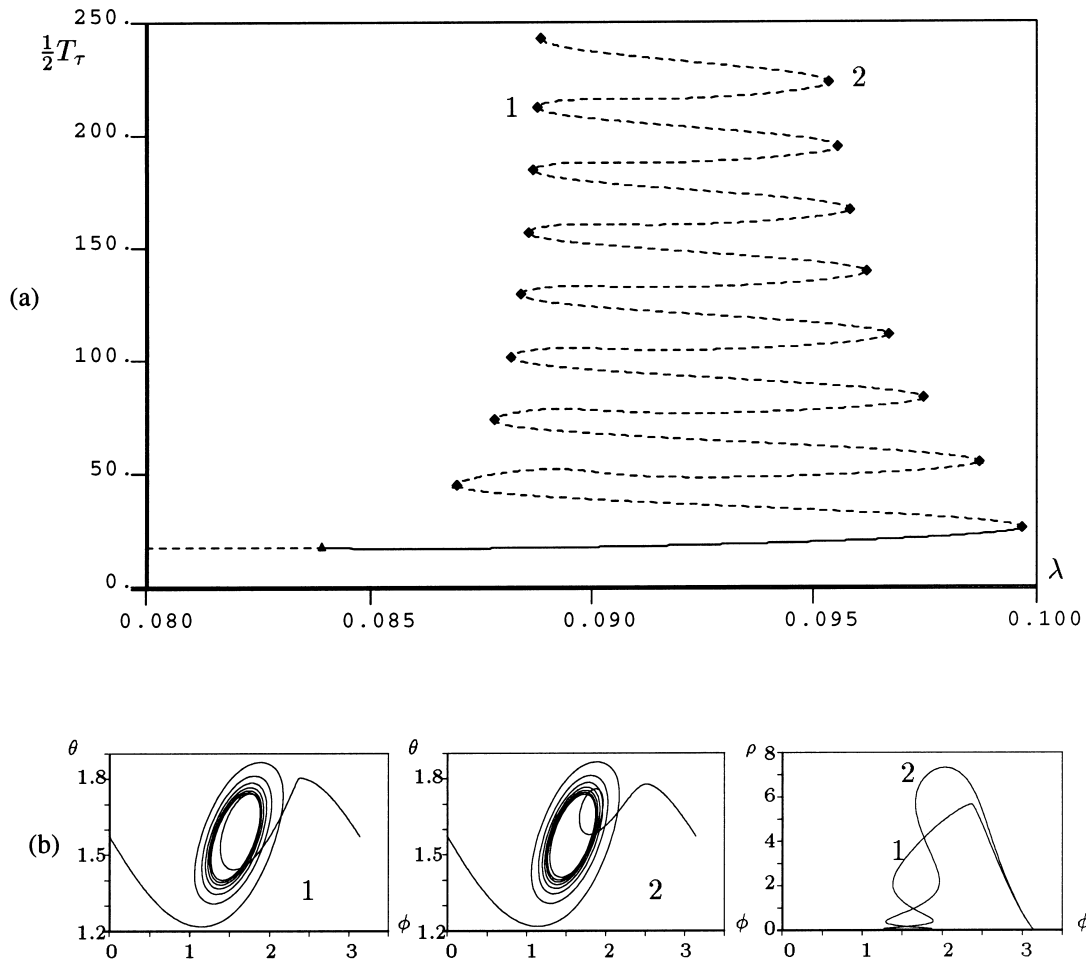


Fig. 15. (a) The period  $T_\tau/2$  between successive bursts on the  $w_c^1$  branch as a function of  $\lambda$ . (b) Trajectories for the points labeled 1 and 2 in (a). These approximate the two distinct heteroclinic cycles between the infinite amplitude fixed points  $u_\infty$  and the infinite amplitude periodic solutions  $qp_\infty$ , cf. Fig. 5, with  $\lambda \equiv \lambda_{c1} \approx 0.089$  and  $\lambda \equiv \lambda_{c2} \approx 0.095$ .

the  $u$  solutions are subcritical, the  $v$  and  $w$  solutions are supercritical, but the  $ns$  and  $qp$  solutions are now both absent. Application of the parameter symmetry  $P_3 \cdot P_1$  and a rescaling of time brings these parameters into the range  $-3 < B_R < -1$ ,  $C_R = -1$  and region  $IV_w$  of parameter space, i.e., to case (a) of Fig. 2. In the original parameters, this translates to the possibility of a heteroclinic cycle involving the  $u_\infty$  and  $v_\infty$  solutions. The bifurcation diagram for  $\Delta\lambda = 0.03$ ,  $\Delta\omega = 0.02$  is shown in Fig. 16 and includes (a) a heteroclinic cycle involving the infinite amplitude  $u_\infty$  and  $v_\infty$  solutions near  $\lambda = 0.08461$  (see Fig. 17), and (b) global bifurcations involving finite amplitude fixed points. Because of the periodicity in  $\phi$  the heteroclinic network consists of two basic units, as illustrated in Fig. 18. This is because on arriving at  $u_\infty$  a trajectory can go, within  $\Sigma$ , to either of two  $v_\infty$  fixed points that are related by periodicity in  $\phi$ . In fact, since the trajectory out of  $\Sigma$  is the same for both units as sketched in Fig. 18(c) and (d), the periods along the  $u/v^1$  and  $w_c^1$  branches become infinite at the *same*  $\lambda$  value. Subsidiary heteroclinicities, sketched in Fig. 19, are also present but form at different  $\lambda$  values.

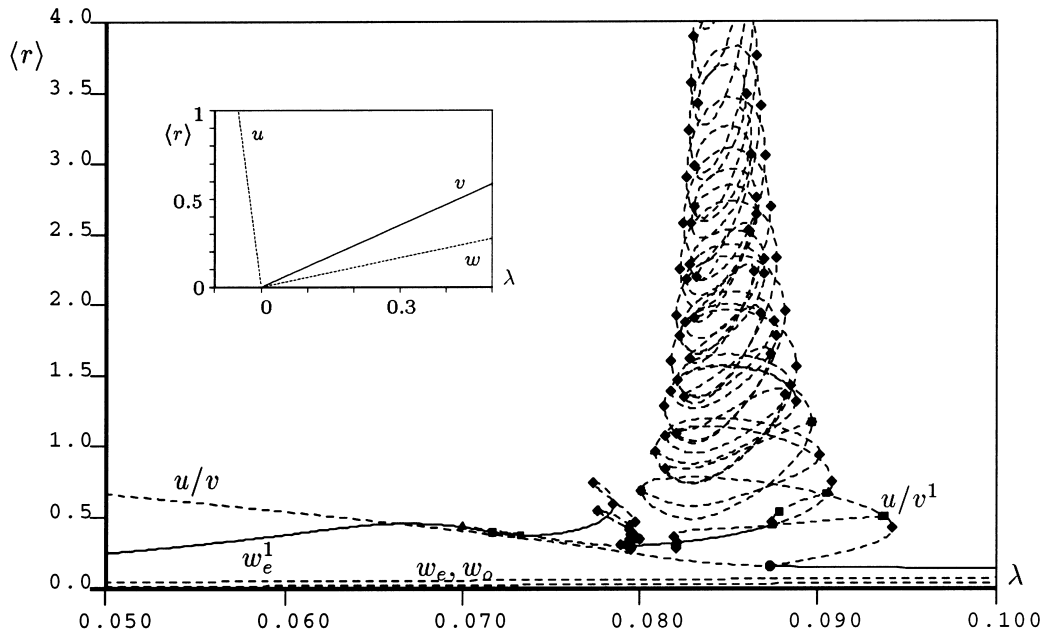


Fig. 16. Bifurcation diagram for the parameters  $A = 1 - 1.5i, B = -2.8 + 5i, C = 0.9 + i, \Delta\lambda = 0.03, \Delta\omega = 0.02$  for comparison with Fig. 14. Not all period-doubled branches are shown. The inset shows the corresponding bifurcation diagram for the perfect system.

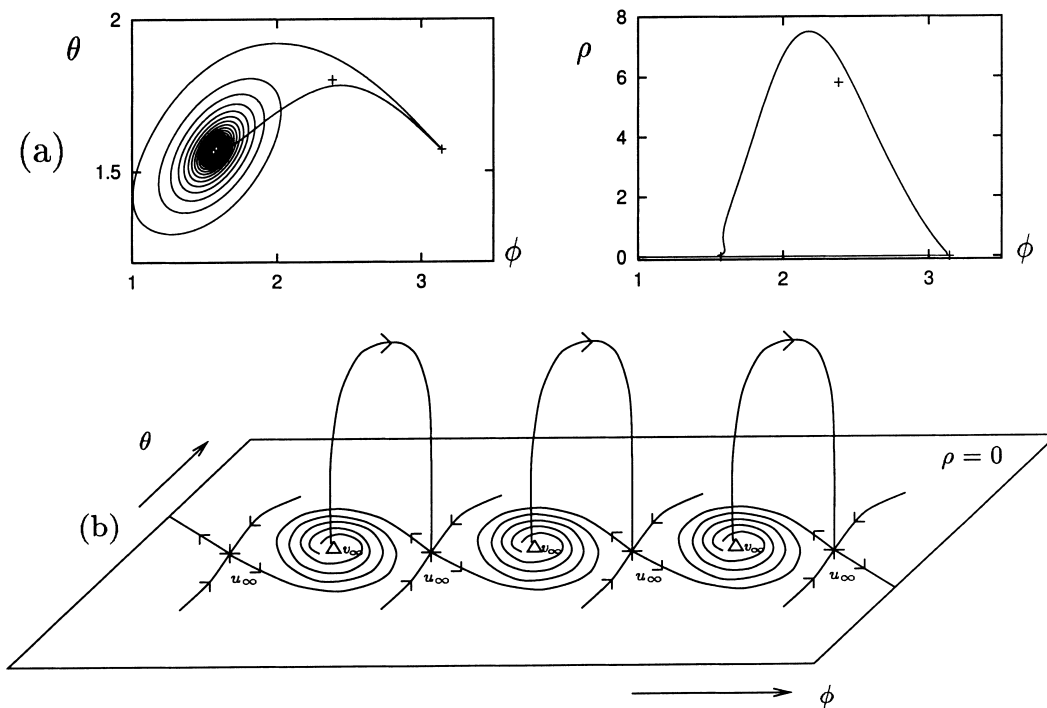


Fig. 17. (a) A numerically calculated heteroclinic cycle involving the infinite amplitude fixed points  $u_\infty$  and  $v_\infty$  at  $\lambda = 0.08461$ . (b) Sketch of the complete heteroclinic network showing all connections.

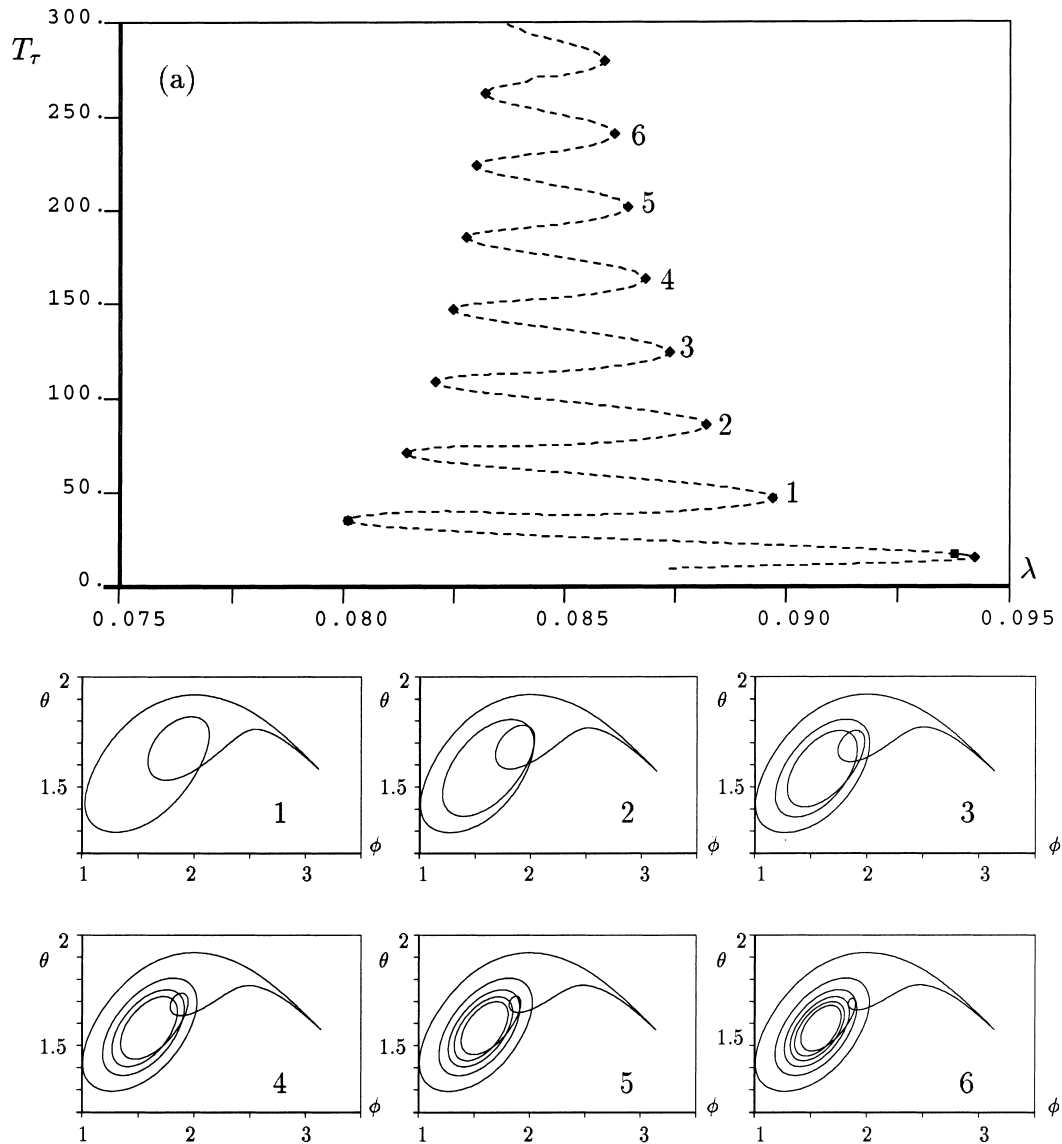


Fig. 18. (a) The  $u/v^1$  and (b) the  $w_c^1$  solution branches as a function of  $\lambda$ . The time between successive bursts in terms of the  $\tau$  time is  $T_\tau$  ( $T_\tau/2$ ) for the  $u/v^1$  ( $w_c^1$ ) branch. The accompanying phase space projections show the approach to the two basic units of the heteroclinic network, sketched in (c) and (d) as solid lines. The cycle forms at  $\lambda_c = 0.08461$ .

It is also possible to find global bifurcations which involve one or both of the  $u/v$  fixed points. For example, for  $\lambda = 0.08208$  there are two  $\kappa_1$ -related homoclinic orbits to  $\kappa_1$ -related  $u/v$  fixed points, while for  $\lambda = 0.0795$  there is a RS heteroclinic orbit connecting the two  $u/v$  fixed points. Fig. 20 shows the eigenvalues  $s_1, s_2, \bar{s}_2$  for the  $u/v$  fixed points for the  $\lambda$  range of interest; both of these global bifurcations occur with  $|\text{Re}(s_2)/s_1| < 1$ , so Shil'nikov-like behavior occurs (but with time reversed from the case which is typically studied because  $\text{Re}(s_2) > 0$ ) [22,20]. We have located a solution branch (which we call the  $s^1$  branch) which terminates at both ends in the global bifurcation at  $\lambda \approx 0.0795$  (see Fig. 21).

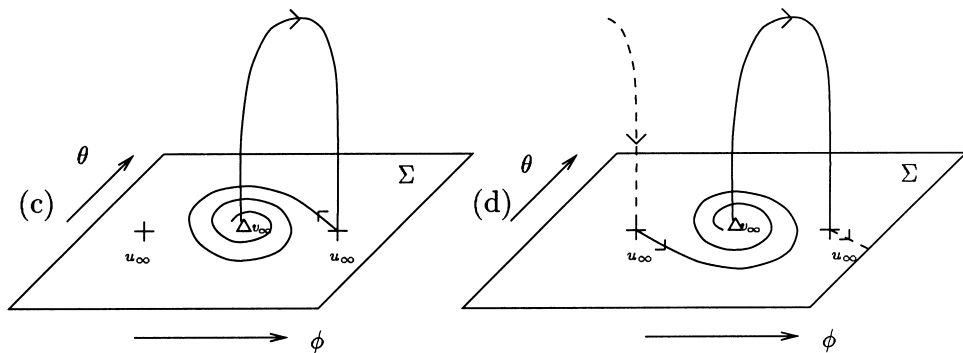
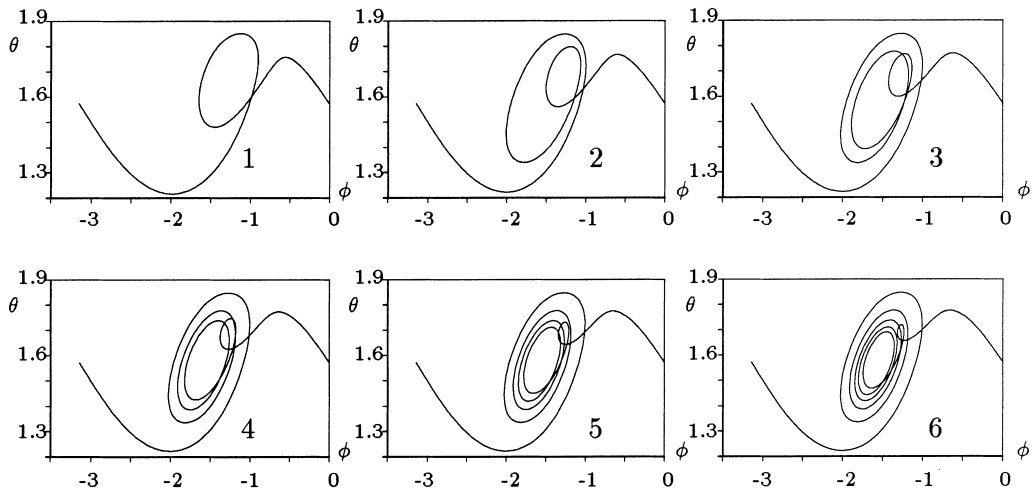
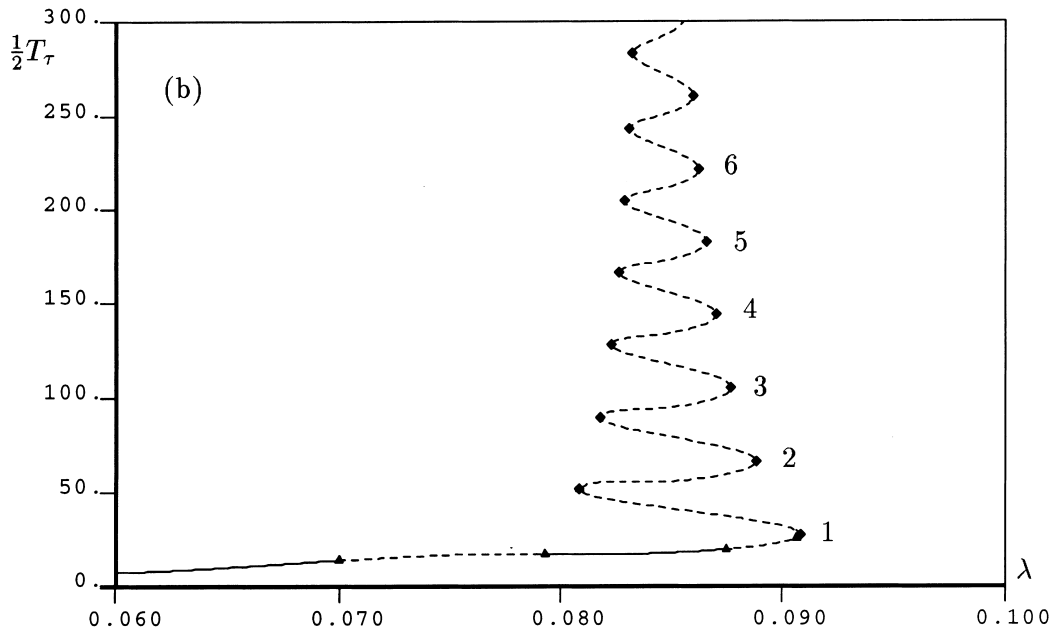


Fig. 18. (Continued).

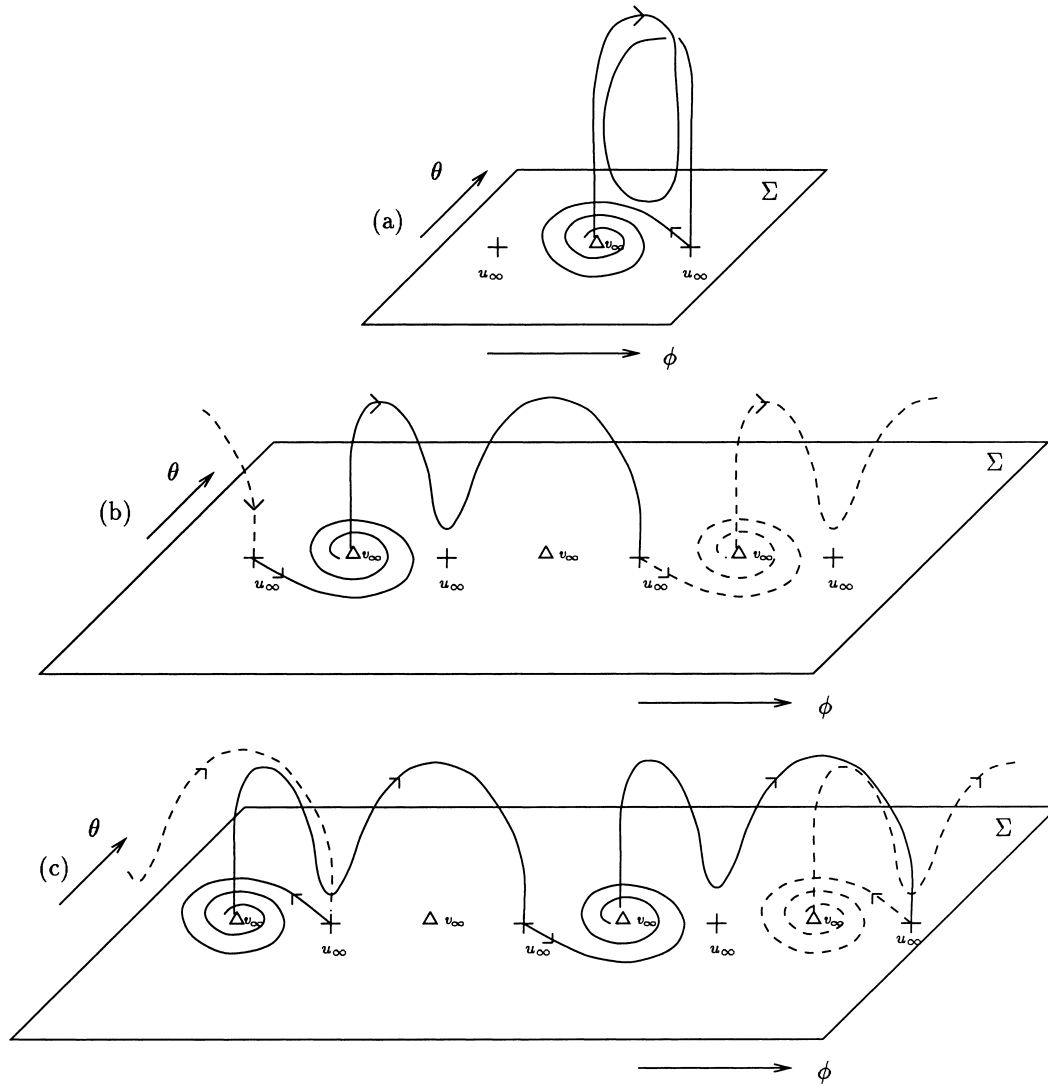


Fig. 19. Sketches of several subsidiary heteroclinic cycles arising from a period-doubling bifurcation on (a) the  $u/v^1$  branch and (b) the  $w_\epsilon^1$  branch, respectively; (c) shows a further possibility not detected numerically. Solid lines indicate the basic units for each cycle.

#### 4.3.4. Example 3

When

$$A = 1 - 1.5i, \quad B = -2.8 + 5i, \quad C = 1 + 0.92i, \quad \Delta\lambda = \Delta\omega = 0$$

the  $u$  and  $ns$  solutions are subcritical, and the  $v$ ,  $w$  and the  $qp$  solutions are supercritical. Application of the parameter symmetry  $P_2$  and a rescaling of time brings these parameters into the range  $-3 < B_R < -1$ ,  $C_R = -1$  and region II of parameter space, i.e., case (d) of Fig. 2. The bifurcation diagram for  $\Delta\lambda = 0.03$ ,  $\Delta\omega = 0.02$  is shown in Fig. 22(a). In this example the  $w_\epsilon^1$  branch undergoes Shil'nikov-like behavior with the saddle-node bifurcations clearly accumulating at two different  $\lambda$  values  $\lambda_{c1} \approx 0.1047$  and  $\lambda_{c2} \approx 0.1181$ ; see Fig. 22(b). Also, the branches which arise from symmetry-breaking pitchfork bifurcations from the  $w_\epsilon^1$  branch do not form subsidiary

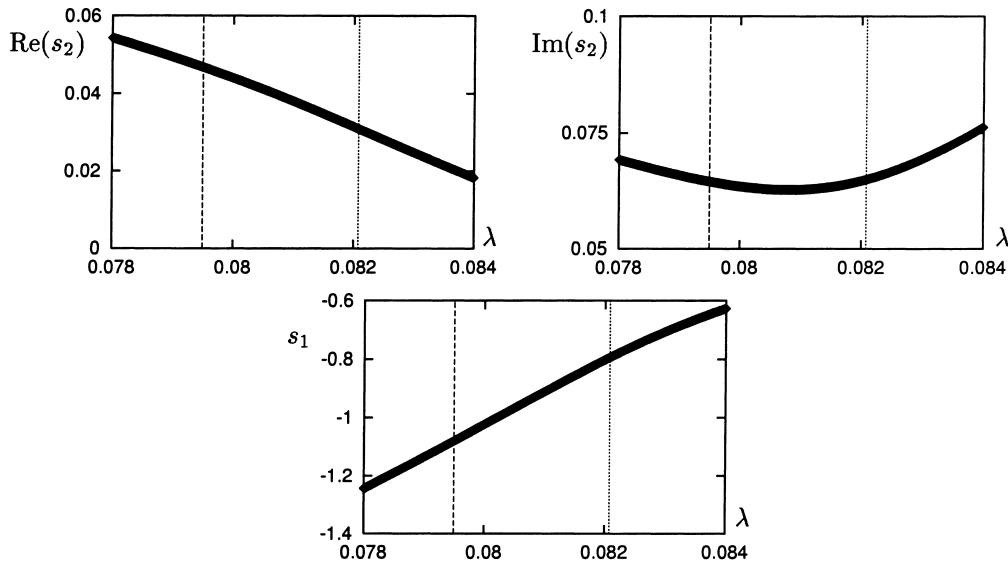


Fig. 20. The eigenvalues  $s_1, s_2, \bar{s}_2$  of the  $u/v$  fixed points as a function of  $\lambda$ . The vertical dashed (dotted) lines show the  $\lambda$  values at which the heteroclinic (homoclinic) bifurcations involving the finite amplitude  $u/v$  fixed points occur.

heteroclinicities (see Fig. 22(c)). In addition, the  $u/v^1$  branch now terminates in a global bifurcation involving the  $u/v$  solutions; numerically, this occurs at the point at which the  $u/v$  solutions undergo a saddle-node bifurcation.

#### 4.3.5. Example 4

When

$$A = 1 - 1.5i, \quad B = -2.8 + 4.5i, \quad C = 0.93 + 0.94i, \quad \Delta\lambda = \Delta\omega = 0$$

the  $u$  and  $ns$  solutions are subcritical, the  $v$  and  $w$  solutions supercritical, and  $qp$  solutions absent. Application of the parameter symmetry  $P_3 \cdot P_1$  and a rescaling of time brings these parameters into the range  $-3 < B_R < -1, C_R = -1$  and region III of parameter space and hence case (b) of Fig. 2. The bifurcation diagram for  $\Delta\lambda = 0.03, \Delta\omega = 0.02$  is shown in Fig. 23. The  $w_e^1$  branch again exhibits Shil'nikov-like behavior, as do the branches born in symmetry-breaking pitchfork bifurcations on the  $w_e^1$  branch (only one such branch is shown in Fig. 23). For the  $\lambda$  values studied, the  $u/v$  branch does not undergo a Hopf bifurcation and no  $u/v^1$  branch is present.

We conclude our brief survey of the dynamics of Eqs. (1) and (2) by listing the eigenvalues and Floquet multipliers for the infinite amplitude solutions involved in heteroclinic cycles for the above examples (see Table 5). In the next section we discuss the effects of changing the magnitude of the forced symmetry-breaking and, given the large amplitude of the bursts, of including higher order terms in these equations.

## 5. Robustness of results

### 5.1. Symmetry-breaking parameters

We focus on Eqs. (1) and (2) with parameters as in Example 1(a) but different values of  $\Delta\omega$ . The Hopf bifurcation on the  $w_e$  branch that gives rise to the  $w_e^1$  solution occurs when

$$2\lambda + (2A_R + B_R)r_{w_e} = 0$$

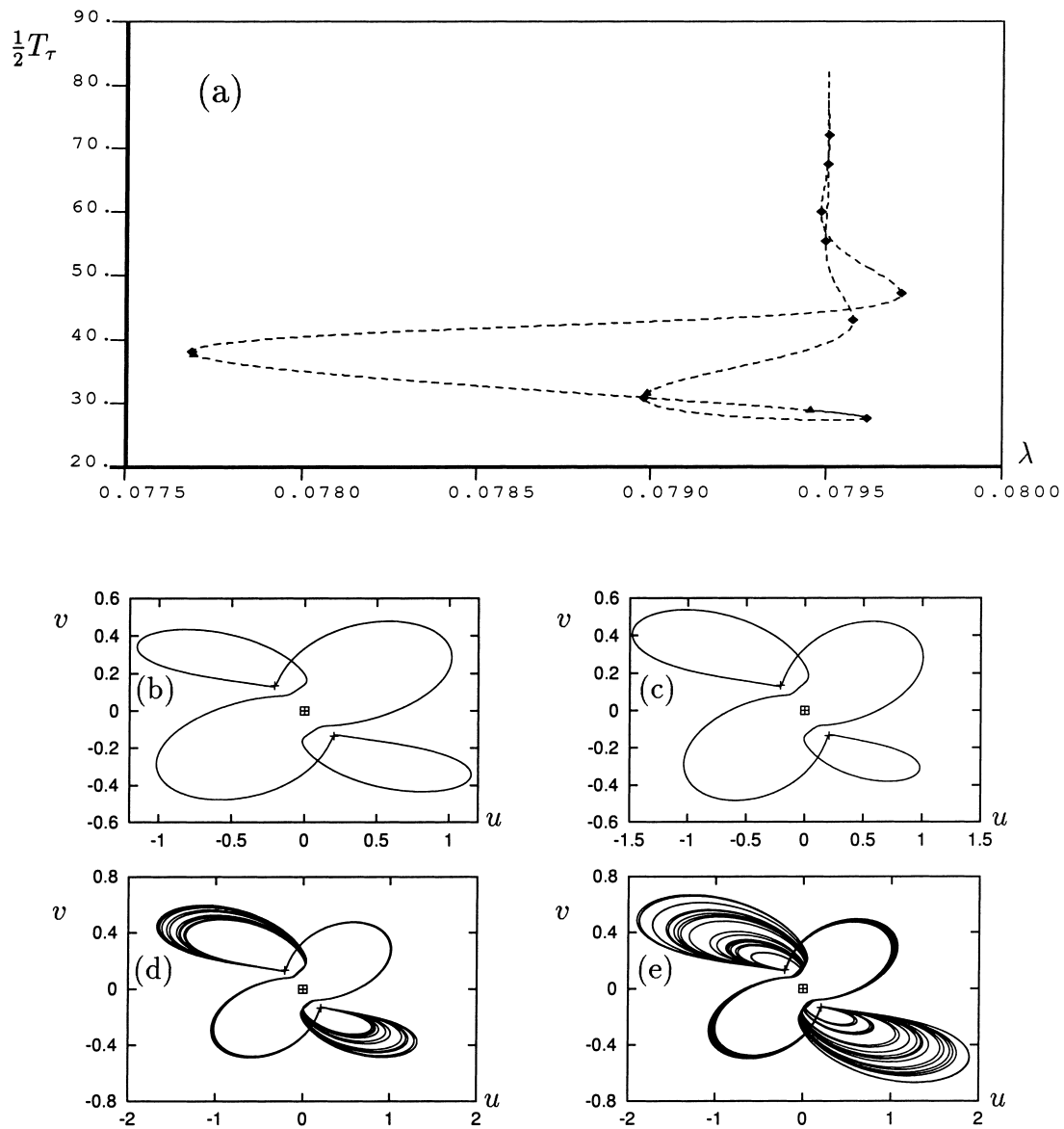


Fig. 21. (a) Bifurcation diagram for the  $s^1$  solution branch. This branch terminates at both ends in the global bifurcation at  $\lambda \approx 0.0795$ . Branches which bifurcate from the  $s^1$  branch in symmetry-breaking pitchfork bifurcations are not shown. (b) Stable RS  $s^1$  solution at  $\lambda = 0.0795$  with  $T_\tau/2 \approx 28.7$ . (c) Stable NRS periodic orbit at  $\lambda = 0.0794$ , arising from a symmetry-breaking pitchfork bifurcation on the  $s^1$  branch at  $\lambda = 0.07945762$ . (d) One of the NRS strange attractors at  $\lambda = 0.07935$ . (e) A RS strange attractor at  $\lambda = 0.0793$  produced from two  $\kappa_1$ -related NRS attractors in a symmetry-increasing bifurcation at  $\lambda = 0.0793499$ .

provided

$$\begin{vmatrix} 2\lambda + (2A_R + B_R + C_R)r_{w_e} & -2\Delta\omega - (B_I + C_I)r_{w_e} \\ 2\Delta\omega + (B_I - C_I)r_{w_e} & 2\lambda + (2A_R + B_R - C_R)r_{w_e} \end{vmatrix} > 0.$$

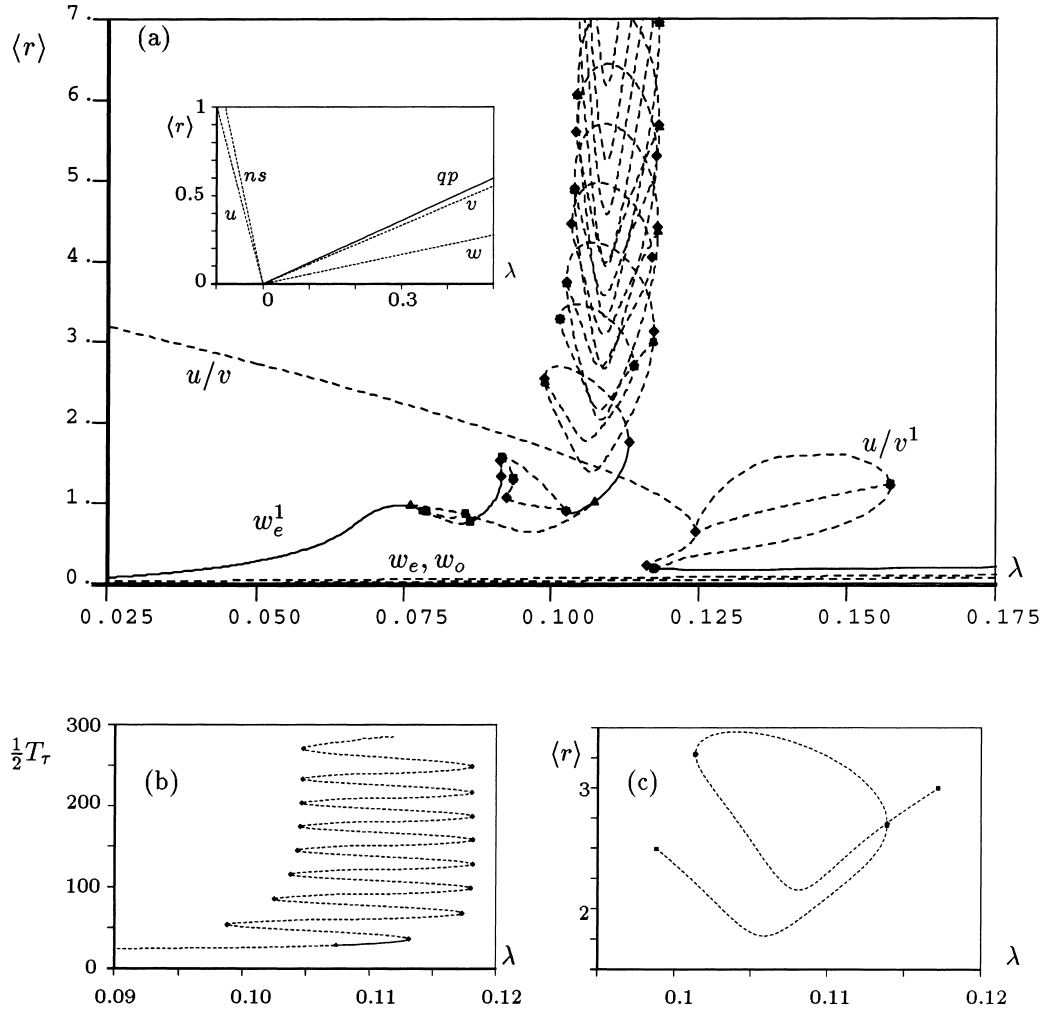


Fig. 22. (a) Bifurcation diagram for the parameters  $A = 1 - 1.5i, B = -2.8 + 5i, C = 0.92 + i, \Delta\lambda = 0.03, \Delta\omega = 0.02$ . Not all period-doubled branches are shown. The inset shows the corresponding bifurcation diagram for the perfect system. (b) Shil'nikov-like behavior on the  $w_e^1$  branch with saddle-node bifurcations accumulating at  $\lambda_{c1} \approx 0.1047$  and  $\lambda_{c2} \approx 0.1181$ . (c) The branch arising from a symmetry-breaking bifurcation on the  $w_e^1$  branch at  $\lambda = 0.09878, \langle r \rangle = 2.545$ , terminating at  $\lambda = 0.1173, \langle r \rangle = 3.001$ .

Here  $r_{w_e}$  is given by (11). Thus  $\Delta\omega$  does not affect the location of this bifurcation which continues to occur at  $\lambda = 0.00857143$ , although it does affect the resulting Hopf frequency. Bifurcation diagrams for  $\Delta\omega = 0.1$  and  $\Delta\omega = 0.5$  are shown in Fig. 24. We see that the  $w_e^1$  branch still terminates at a global bifurcation involving the finite amplitude  $u/v$  solutions; however, this occurs at higher  $\lambda$  values than for  $\Delta\omega = 0.02$ . Moreover, the  $u/v^1$  solutions no longer exist. As  $\Delta\omega$  increases the phase  $\phi$  slips more and more rapidly, cf. Eq. (5), and averaging then eliminates the parameter  $C$  from Eqs. (3) and (4), giving

$$r = -\frac{2\lambda}{2A_R + B_R}, \quad \theta = \cos^{-1}\left(-\frac{2\Delta\lambda}{rB_R}\right).$$

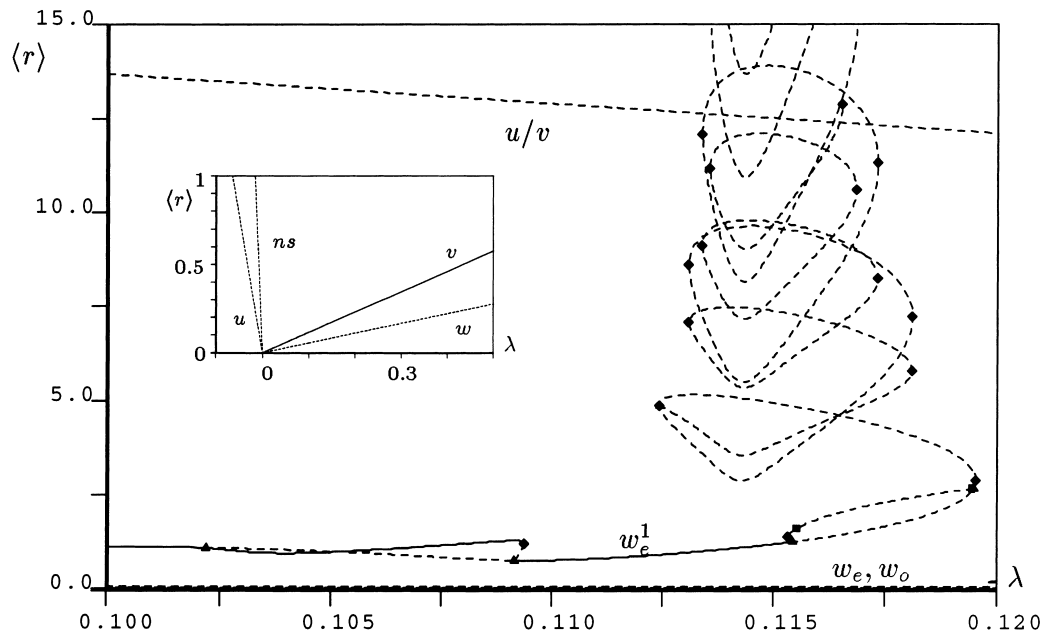


Fig. 23. Bifurcation diagram for the parameters  $A = 1 - 1.5i$ ,  $B = -2.8 + 4.5i$ ,  $C = 0.93 + 0.94i$ ,  $\Delta\lambda = 0.03$ ,  $\Delta\omega = 0.02$ . Not all period-doubled branches are shown. The inset shows the corresponding bifurcation diagram for the perfect system.

Since  $r$  is now constant in time the bursts fade away with increasing  $\Delta\omega$  and are replaced by smaller amplitude, higher frequency states (see Table 6). However, even for extreme values of  $\Delta\omega$  it is apparently still possible to choose  $\lambda$  values so that bursts of large dynamic range occur (see Fig. 25).

We next consider the parameters of Example 1(a) but with  $\Delta\omega = -0.02$ . The resulting bifurcation diagram is shown in Fig. 26. Both  $w_e^1$  and  $u/v^1$  branches undergo Shil'nikov-like behavior, with the saddle-node bifurcations accumulating to  $\lambda_{c1} \approx 0.02554$  and  $\lambda_{c2} \approx 0.03642$ . New types of solutions found for these parameter values include stable chaotic states which visit the vicinity of the same infinite amplitude fixed point (see Fig. 27(a)) and stable chaotic states which are characterized by successive visits to the vicinity of the  $\Sigma$  subspace sometimes near the *same* and sometimes near a *different* but symmetry-related infinite amplitude fixed point (see Fig. 27(b)), much as already described by Rodriguez and Schell [29].<sup>1</sup> Fig. 27(c) demonstrates that for  $\lambda_{c1} < \lambda < \lambda_{c2}$  two distinct heteroclinic cycles exist for the *same*  $\lambda$  value, as expected from Section 4.2.

When  $\Delta\omega$  is held fixed instead bursts persist for a range of  $\Delta\lambda$  values as well. However, we have not attempted a detailed classification of the properties of Eqs. (1) and (2) for arbitrary values of  $\Delta\lambda$  and  $\Delta\omega$ .

## 5.2. Higher order terms

Thus far we have studied Eqs. (1) and (2) which have been truncated at third order in the amplitudes  $z_+$  and  $z_-$ . The presence of bursts of large amplitude requires, however, that we reexamine the truncation that led us to these equations. Recall that in the derivation that leads to these equations the *physical* amplitudes are  $\epsilon^{1/2}z_{\pm}$ , where  $\epsilon$  measures the distance above threshold. It follows that the physical amplitudes remain small provided

<sup>1</sup> The term  $-0.75r_1^3$  in Eq. (4b) of [29] should be  $-0.75r_1^3\rho$ .

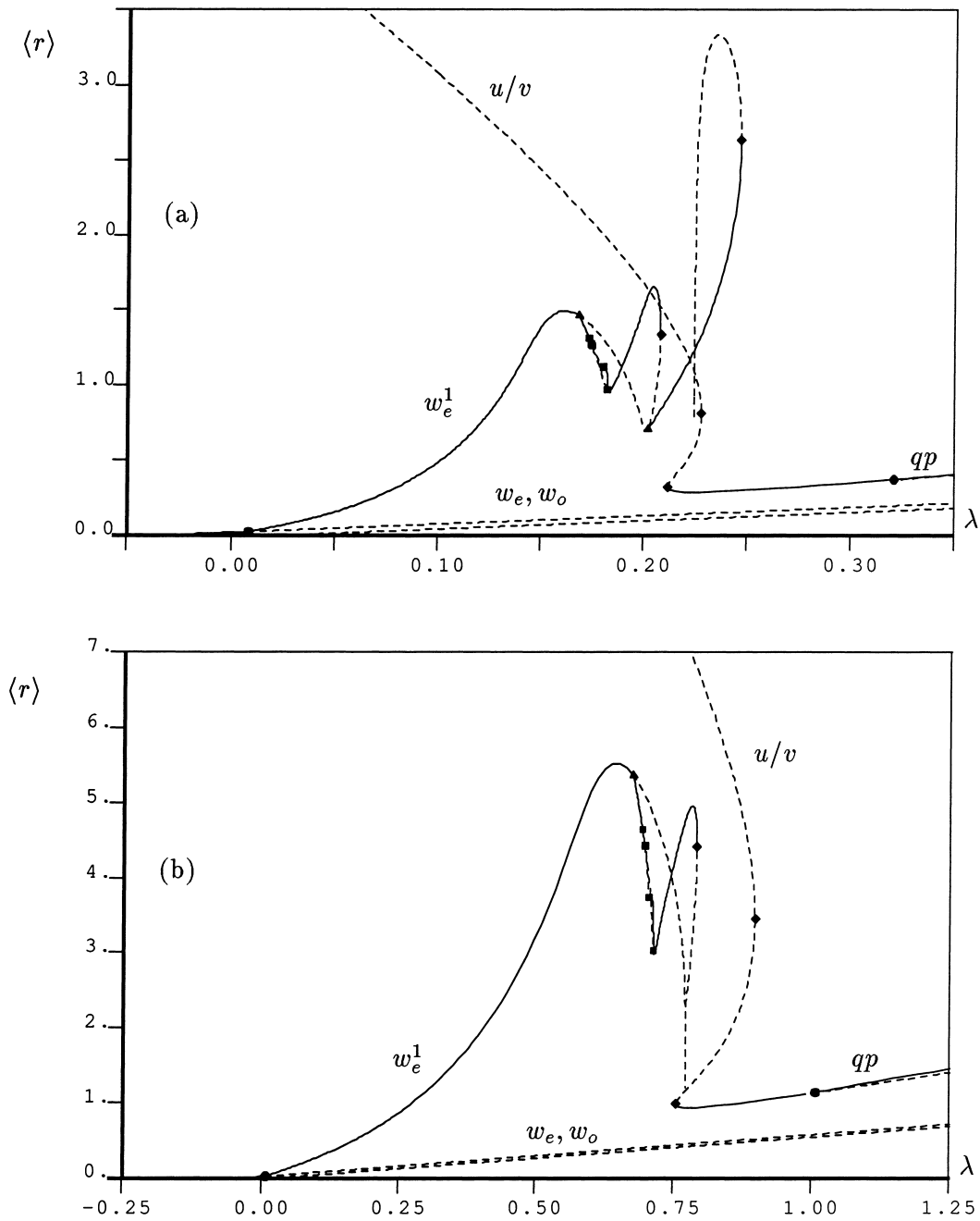


Fig. 24. Bifurcation diagrams for the parameters  $A = 1 - 1.5i, B = -2.8 + 5i, C = 1 + i, \Delta\lambda = 0.03$  and (a)  $\Delta\omega = 0.1$ , (b)  $\Delta\omega = 0.5$ .

$\epsilon^{1/2}|z_{\pm}|_{\max} \ll 1$ . Under these conditions all fifth-order terms in Eqs. (1) and (2) enter the derivation with  $\mathcal{O}(\epsilon)$  coefficients and remain small relative to the cubic terms retained. However, the presence of even small fifth-order terms has an effect: if such terms are stabilizing the solutions responsible for the bursting behavior cannot reach arbitrarily large amplitude and instead have large but *finite* amplitudes. As an example we consider

Table 6

Maximum burst amplitude ( $r_{\max}$ ) and time between bursts ( $T_b$ ) for stable periodic solutions when  $A = 1 - 1.5i, B = -2.8 + 5i, C = 1 + i, \lambda = 0.1, \Delta\lambda = 0.03$ , and different values of  $\Delta\omega$

$\Delta\omega$	$r_{\max}$	$T_b$
0.02	7.649	29.27
0.1	0.763	7.85
0.5	0.296	2.69

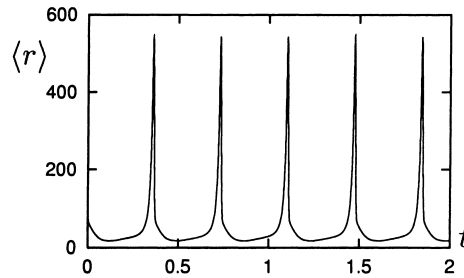


Fig. 25. Bursts with large dynamic range at  $\lambda = 15$  and  $A = 1 - 1.5i, B = -2.8 + 5i, C = 1 + i, \Delta\lambda = 0.03$  and  $\Delta\omega = 10$ .

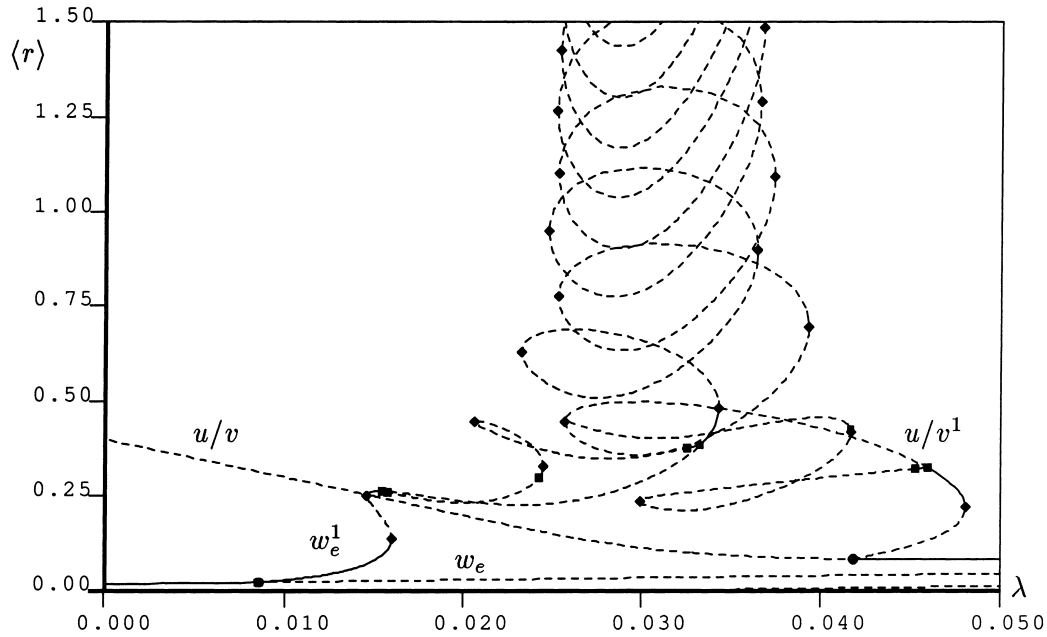


Fig. 26. Bifurcation diagram for the parameters  $A = 1 - 1.5i, B = -2.8 + 5i, C = 1 + i, \Delta\lambda = 0.03, \Delta\omega = -0.02$ . The bifurcation diagram for the perfect system is shown in the inset of Fig. 3.

the system

$$\dot{z}_+ = [\lambda + \Delta\lambda + i(\omega + \Delta\omega)]z_+ + A(|z_+|^2 + |z_-|^2)z_+ + B|z_+|^2z_+ + C\bar{z}_+z_-^2 + D|z_+|^4z_+,$$

$$\dot{z}_- = [\lambda - \Delta\lambda + i(\omega - \Delta\omega)]z_- + A(|z_+|^2 + |z_-|^2)z_- + B|z_-|^2z_- + C\bar{z}_-z_+^2 + D|z_-|^4z_-$$

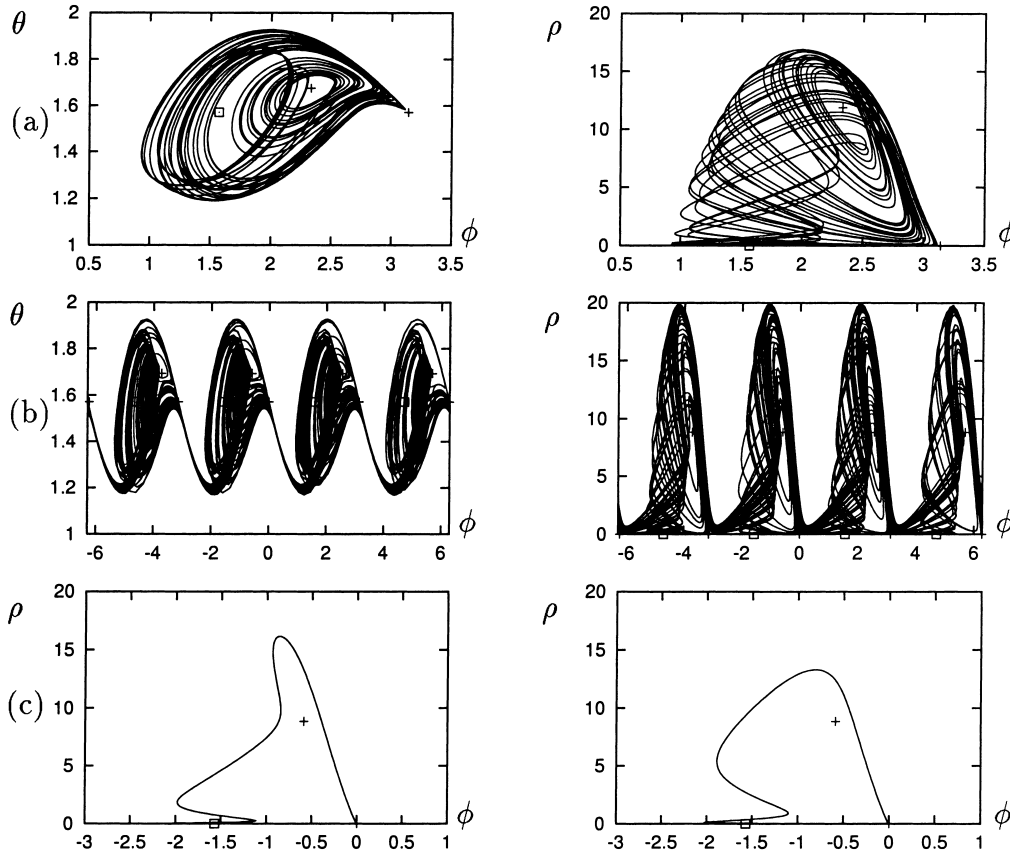


Fig. 27. (a) Stable chaotic state with repeated visits to the vicinity of the same infinite amplitude states for  $A = 1 - 1.5i$ ,  $B = -2.8 + 5i$ ,  $C = 1 + i$ ,  $\Delta\lambda = 0.03$ ,  $\Delta\omega = -0.02$  and  $\lambda = 0.04$ . (b) Stable chaotic state at  $\lambda = 0.03$  which makes repeated visits to either the same infinite amplitude state or symmetry-related ones. (c) Two distinct heteroclinic cycles exist for  $\lambda = 0.03$  which lies between  $\lambda_{c1}$  and  $\lambda_{c2}$ .

and analyze the consequences of the new terms, choosing the  $\mathcal{O}(\epsilon)$  coefficient  $D \equiv D_R + iD_I$  such that the subcritical branch undergoes a saddle-node bifurcation. In this case solutions on this branch exist even for  $\lambda > 0$ . Eqs. (13)–(15) become

$$\begin{aligned} \frac{d\rho}{d\tau} &= -\rho[2A_R + B_R(1 + \cos^2\theta) + C_R \sin^2\theta \cos 2\phi] - 2(\lambda + \Delta\lambda \cos\theta)\rho^2 - \frac{5}{4}D_R - \frac{3}{4}D_R \cos 2\theta, \\ \frac{d\theta}{d\tau} &= \sin\theta[\cos\theta(-B_R + C_R \cos 2\phi) - C_I \sin 2\phi] - 2\Delta\lambda \sin\theta\rho - \frac{D_R}{\rho} \cos\theta \sin\theta, \\ \frac{d\phi}{d\tau} &= \cos\theta(B_I - C_I \cos 2\phi) - C_R \sin 2\phi + 2\Delta\omega\rho + \frac{D_I \cos\theta}{\rho}. \end{aligned}$$

We consider the parameter values from Example 2 with  $(D_R, D_I) = \epsilon(-1, 1)$  and focus our discussion on the  $u/v^1$  branch; similar results hold for other branches. When  $\epsilon = 0.01$  the  $u_\infty$  fixed points have moved out of the  $\rho = 0$  plane which is no longer invariant; we call these  $u_{\text{finite}}$  fixed points. For example, when  $\lambda = 0.1$  the coordinates of  $u_{\text{finite}}$  are  $(\rho, \theta, \phi) = (0.0460, 1.5770, -0.0136 + m\pi)$ , where  $m$  is an integer. Fixed points analogous to the  $v_\infty$  fixed points do not exist for these parameters. Bursts now occur when the trajectory makes visits near the large

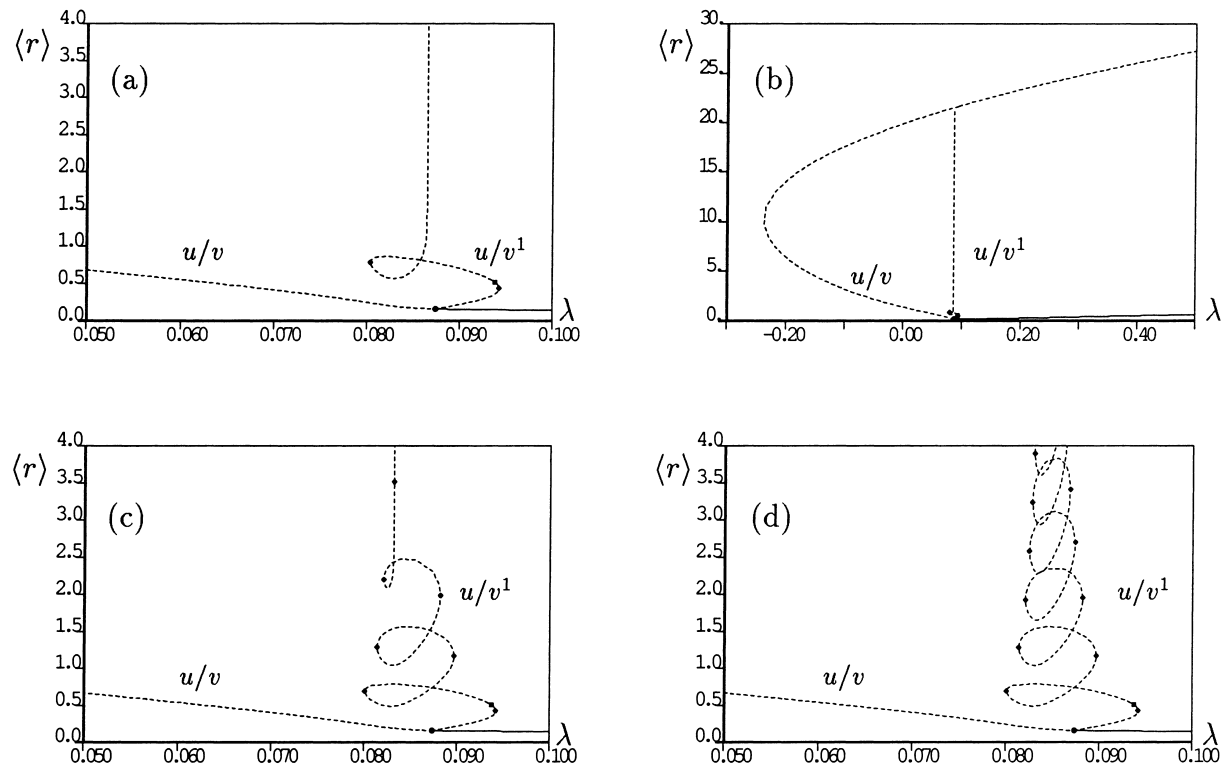


Fig. 28. Bifurcation diagrams for the  $u/v^1$  branch for (a,b)  $\epsilon = 0.01$ , (c)  $\epsilon = 0.00001$ , and (d)  $\epsilon = 0$ . For  $\epsilon > 0$  the  $u/v^1$  solution collides with a new  $u_{\text{finite}}$  fixed point; this global bifurcation manifests itself as a vertical branch in the bifurcation diagrams. At the same time  $\langle r \rangle$  approaches the value of  $r$  for the new fixed point.

but finite amplitude  $u_{\text{finite}}$  fixed points. Fig. 28 compares the bifurcation diagrams for  $\epsilon = 0.01$ ,  $\epsilon = 0.00001$  and  $\epsilon = 0$ , and demonstrates that as  $\epsilon$  decreases the system behavior approaches that for  $\epsilon = 0$ , i.e., the limit  $\epsilon \rightarrow 0$  captures the mechanism responsible for the generation of bursts near threshold of the primary instability. Moreover, in this example, the “complexity” of the dynamical behavior increases with decreasing  $\epsilon$ , in contrast with typical situations in the study of the transition to complex behavior where the “complexity” of a system increases with the distance above threshold.

Finally, it should also be noted that when  $\rho$  is small any  $D_4$ -breaking terms omitted from the cubic terms in Eqs. (1) and (2) may also become significant and change the detailed dynamics near  $\rho = 0$ .

## 6. Conclusion

In this paper we described a simple geometrical mechanism responsible for the presence of bursts, both periodic and nonperiodic, very close to threshold of an oscillatory instability in systems with broken  $D_4$  symmetry. The mechanism relies on the presence of structurally stable connections in an invariant subspace  $\Sigma$  corresponding to infinite amplitude states together with a connection  $\Sigma$  to  $\Sigma$  and is of codimension one.

This geometrical picture is not specific to this system, although the presence of exact  $D_4$  symmetry in this subspace greatly facilitates the analysis. Indeed, in the context of near Hamiltonian systems with an indefinite Hamiltonian

a related scenario was suggested already by Newell et al. [30,31]. In fact any dynamical system on  $R^N$  with an invariant subspace  $\Sigma$  that contains at least two invariant sets  $A$  and  $B$ , one of which ( $B$ ) is nonstable in  $\Sigma$  and the other ( $A$ ) attracting in  $\Sigma$  can generate this type of mechanism provided that  $B$  is attracting and  $A$  nonstable in  $R^N \setminus \Sigma$ . If the unstable manifold of  $A$  is one-dimensional the resulting mechanism will be of codimension one and hence readily observable. Note that neither  $A$  nor  $B$  need to be chaotic in order that the resulting dynamics be chaotic. This type of set-up, discussed already by Knobloch and Moore [32,33], has much in common with recent studies of on–off and in–out intermittency [34,35] but differs in several respects. In on–off intermittency a strange attractor in an invariant space  $\Sigma$  loses stability in the transverse direction when a parameter  $\lambda$  is varied but the dynamics in  $\Sigma$  do not depend on  $\lambda$ . This is so for our infinite amplitude states although in our case the dynamics in  $\Sigma$  are simple. In in–out intermittency there may be several invariant sets in  $\Sigma$ , possibly nonchaotic, with different transverse stability properties all of which vary with the parameter  $\lambda$ . The bursts that result do not require per se proximity to a heteroclinic connection (although such a bifurcation is inevitably in the background) and hence have a finite dynamic range determined by the global reinjection mechanism. The resulting bursts are therefore of finite duration. Our scenario differs in that the bursts are associated with visits to the invariant subspace, not away from it, and have arbitrarily large dynamic range. Moreover the bursts have finite duration despite their association with a heteroclinic cycle. In addition our problem has the skew product structure of on–off intermittency but chaotic bursts are produced despite the absence of a chaotic attractor in  $\Sigma$ . Because of these differences we were able to study explicitly the sequence of bifurcations responsible for the generation of the bursts. Moreover, because the existence of the bursts is a consequence of weak breaking of the  $D_4$  symmetry our bursts occur very close to onset of the oscillatory instability, and their presence can therefore be viewed as a *manifestation* of forced symmetry-breaking. However, the dynamics of the system without forced-symmetry breaking are still crucial for understanding the dynamics in the imperfect system. We have seen that as the magnitude of the symmetry breaking is increased for fixed  $\lambda$  the bursts decrease in amplitude and increase in frequency. It appears, however, that some type of bursting remains in appropriate ranges of  $\lambda$  values further from threshold. As in other problems of this type forced symmetry-breaking has a particularly dramatic effect when both supercritical and subcritical branches are present.

The mechanism we have described finds a number of natural applications in physical systems of interest. This is because broken  $D_4$  symmetry can arise in several different ways. The most straightforward is in systems with approximate square geometry undergoing an oscillatory instability. As examples we mention three-dimensional overstable convection (such as binary fluid convection) in containers of nearly square cross-section [36,37] and more generally any partial differential equation on a nearly square domain describing the evolution of an oscillatory instability (cf. [38]). Other systems where such equations arise are four coupled oscillators with nearly identical coupling [10,39,40] and the related problem of spring-supported fluid-conveying tubes [41].

Broken  $D_4$  symmetry also arises in slender systems undergoing an oscillatory instability. If such a system has left–right reflection symmetry (the symmetry  $\kappa_1$ ) the first modes that set in typically have opposite parity. Moreover, because the neutral stability curve for the unbounded system usually has a parabolic minimum these set in in close succession as the bifurcation parameter is increased. Since, as first argued in [11], the equations for the formally infinite system cannot distinguish between these two modes, the amplitude equations must in this limit also be equivariant with respect to mode interchange (the symmetry  $\kappa_2$ ). Since in any finite domain the two modes do not generically set in simultaneously the  $D_4$  symmetry generated by  $\kappa_1$  and  $\kappa_2$  is inevitably broken. The resulting bursts take the form of either blinking states (rotations) or winking states (librations) and bear substantial resemblance to the bursts observed in binary fluid convection very close to threshold [42] as discussed in [12]. Systems featuring competition between two nearly degenerate oscillatory modes form a further class of systems to which the present mechanism is likely to be relevant. As examples we mention the Faraday system in a nearly square container [43], and models of the solar magnetic cycle [44,45]. Finally, since the normal form for a Hopf bifurcation with the

symmetry of the quaternion group is identical to the normal form for a Hopf bifurcation with  $D_4$  symmetry [46], bursts might also occur in systems with weakly broken quaternion symmetry.

### Acknowledgements

This work was supported in part by the NSF under grant DMS-9703684 and NASA under grant NAG3-2152. We thank E. Doedel for assistance with AUTO.

### Appendix A. Parameter symmetries

Suppose that the original parameters do not lie in the wedge in parameter space given by  $3C_R < B_R < C_R$ ; then it is possible to act with parameter symmetries to bring the parameters into this wedge with the phase space suitably relabeled. Time may then be rescaled so that  $C_R = -1$ . The existence and stability results in the main text for solutions with  $-3 < B_R < -1$  and  $C_R = -1$  may then be applied to the transformed system. By “undoing” the relabeling of phase space we can deduce the existence and stability properties for the original parameters. Note that care should be used in determining the stability properties because the parameter symmetry  $P_3$  reverses time, thereby changing the signs of the eigenvalues; also, changing the sign of the radial eigenvalue changes subcritical branches into supercritical branches and vice versa. For given values of  $B_R$  and  $C_R$ , Fig. 29 shows the necessary action to bring the parameters into the wedge  $3C'_R < B'_R < C'_R$ . Note that if after this action  $B'_1 > 0$  a further action of  $P_4$  will make  $B'_1 < 0$ , if desired.

We illustrate the use of parameter symmetries with an example. Suppose  $A = 1 - 1.5i$ ,  $B = -2.8 + 5i$ , and  $C = 1 + i$  (the system behavior for these parameters is studied carefully in Example 1(a) of Section 4.3). Since  $B_R = -2.8$ ,  $C_R = 1$ , from Fig. 29 the action  $P_2$  brings the parameters into the desired wedge in parameter space. This gives  $B'_1 > 0$  so we then act with  $P_4$ . Overall

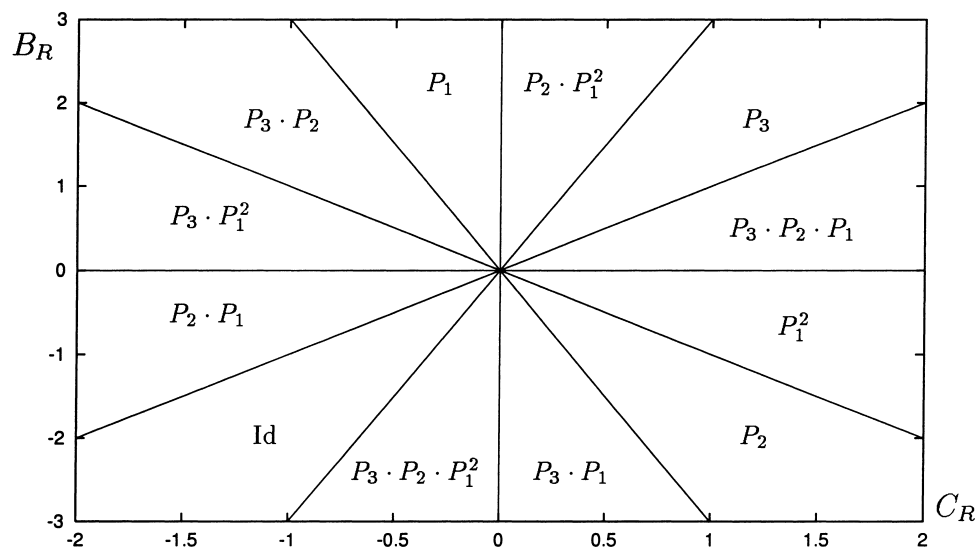


Fig. 29. The parameter symmetries required to transform different regions of the parameter space into the wedge  $3C'_R < B'_R < C'_R$ .

$$P_4 \cdot P_2 : (u, v, w) \rightarrow (v, u, w) \equiv (u', v', w')$$

$$(A, B, C) = (1 - 1.5i, -2.8 + 5i, 1 + i) \rightarrow (1 + 1.5i, -2.8 - 5i, -1 + i) \equiv (A', B', C').$$

Since  $C'_R = -1$  it is not necessary to rescale time to apply the results from the main text. We find (see Fig. 1) that the transformed parameters lie just within region I of parameter space. Letting  $u'$  solutions be fixed point solutions with  $v' = w' = 0$ , etc., we find that the  $u'$ ,  $v'$ , and  $w'$  solutions are, respectively, a source, saddle, and source in the associated spherical system (see Table 3); also the  $v'$  solutions are subcritical and  $u'$  and  $w'$  solutions are supercritical. A supercritical  $qp'$  solution also exists enclosing the  $u'$  solution in the associated spherical system. As an example of “undoing” the relabeling of phase space, consider the  $u'$  solutions. Since these solutions satisfy  $v' = w' = 0$ , in the original parameters they correspond to solutions with  $u = w = 0$ , i.e.,  $v$  solutions. The stability properties of the  $v$  solutions in the original parameters are identical to the stability properties of the  $u'$  solutions in the transformed parameters. We thus conclude that for  $A = 1 - 1.5i$ ,  $B = -2.8 + 5i$ , and  $C = 1 + i$  the  $u$  solution is a subcritical saddle and that the  $v, w$  solutions are supercritical sources. There is also a supercritical  $qp$  libration around the  $v$  solution.

As noted in the main text, the parameter symmetry  $P_1$  applies only if we restrict attention to the reduced phase space  $(u, v, w)$ ; that is, the equation for  $\psi$  is not equivariant under this parameter symmetry. However, this does not affect our use of parameter symmetries to establish the existence and stability properties of new solutions because these depend only on the dynamics in the three-dimensional system from which the  $\psi$  equation decouples.

### Appendix B. Radial stability of $ns$ and $qp$ solutions

For the parameter range  $-3 < B_R < -1$ ,  $C_R = -1$  we can place the following restrictions on the radial stabilities of the  $ns$  and  $qp$  solutions. Recall that these solutions are radially stable (unstable) if they bifurcate supercritically (subcritically) from the trivial state.

- (i) Suppose that  $ns$  solutions exist. If the  $v$  solutions are supercritical, then the  $ns$  solutions must also be supercritical. If the  $w$  solutions are subcritical, then the  $ns$  solutions must also be subcritical.

These results follow from the observations that when  $s_1^v = 0$ , the condition  $s_2^v s_3^v = 0$  is identical to the condition  $s_1^{ns} = 0$ , and similarly, when  $s_1^w = 0$ , the condition  $s_2^w s_3^w = 0$  is identical to the condition  $s_1^{ns} = 0$ . In other words, this says that when  $A_R$  is chosen so that the radial stability of the  $v$  or  $w$  solution is degenerate, the condition for the pitchfork bifurcation which causes the creation or destruction of the  $ns$  solutions is identical to the condition that the radial stability of the  $ns$  solutions is degenerate. Using this result and a numerical study of how the curve  $s_1^{ns} = 0$  varies in  $(B_I, C_I)$  space with  $A_R$ , we verify (i) (see Fig. 30).

- (ii) Suppose  $qp$  solutions exist. If the  $u$  solutions are subcritical then the  $qp$  solutions are also subcritical.

We write

$$\bar{F} = 2A_R + \frac{1}{T_\tau} \int_0^{T_\tau} G(\theta^*(\tau'), \phi^*(\tau')) d\tau' \equiv 2A_R + \bar{G},$$

where

$$G(\theta, \phi) = B_R(1 + \cos^2\theta) + C_R \sin^2\theta \sin 2\phi,$$

and define  $A_R^* = A_R^*(B_R, B_I, C_R, C_I)$  to be the value of  $A_R$  for which  $\bar{F} = 0$  (so that if  $A_R^* > A_R (< A_R)$  the  $qp$  branch is supercritical (subcritical)). Thus,

$$A_R^* = -\frac{\bar{G}}{2}.$$

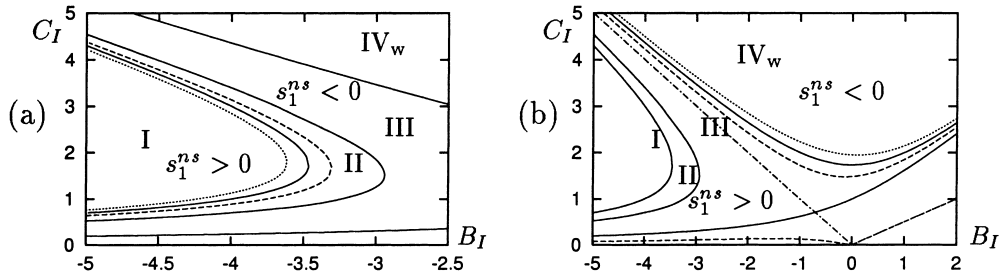


Fig. 30. When  $B_R = -2$ ,  $C_R = -1$  the radial eigenvalue  $s_1$  of the  $v$ ,  $u$  and  $w$  solutions vanishes for  $A_R = 0.5$ ,  $1.5$  and  $2.0$ , respectively. (a) The dotted (dashed) lines show where  $s_1^{ns} = 0$  for  $A_R = 0.4$  ( $0.6$ ). For  $A_R = 0.4$ ,  $s_1^{ns} < 0$  in regions II and III (the only regions in which the  $ns$  solutions exist) and the  $ns$  solutions are always supercritical. For  $A_R = 0.6$  the curve  $s_1^{ns} = 0$  has moved beyond the boundary between regions I and II and the  $ns$  solutions may be supercritical or subcritical depending on the values of  $B_I$  and  $C_I$ . (b) The dot-dashed, dashed, and dotted lines show where  $s_1^{ns}$  switches signs for  $A_R = 1.5$ ,  $1.8$ , and  $2.2$ , respectively. For  $A_R = 1.5$ ,  $s_1^{ns} < 0$  only outside regions I and II. For  $A_R = 1.8$  the  $ns$  solutions may be supercritical or subcritical depending on the values of  $B_I$  and  $C_I$ . For  $A_R = 2.2$  the curve  $s_1^{ns} = 0$  has moved beyond the boundary between regions III and IV<sub>w</sub>; since  $ns$  solutions only exist in regions II and III the  $ns$  solutions are now always subcritical. Similar behavior is found for other values of  $B_R$  in the range  $-3 < B_R < -1$ .

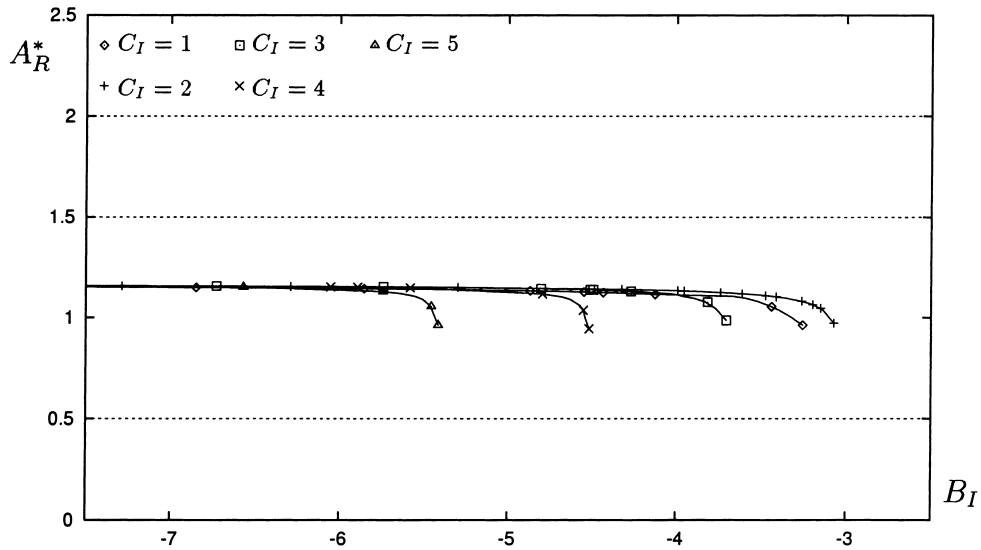


Fig. 31. The dependence of  $A_R^*$  on  $B_I$  for different fixed values of  $C_I$  with  $B_R = -2$  and  $C_R = -1$ . These data points are extracted from the Floquet multipliers calculated by AUTO. For a particular value of  $C_I$ , the maximum value of  $B_I$  is reached when the  $qp$  solution collides with the  $ns$  solutions, corresponding to the boundary between regions II and III. The dotted lines at  $A_R^* = 0.5$ ,  $1.5$ , and  $2.0$  are for the respective  $A_R$  values at which the radial stabilities of the  $v$ ,  $u$ , and  $w$  solutions are degenerate. Similar behavior is found for other values of  $B_R$  in the range  $-3 < B_R < -1$ .

The value of  $\bar{G}$  for a periodic orbit can be calculated by numerical integration or extracted from the Floquet multipliers calculated by AUTO [27]. In Fig. 31 we plot the dependence of  $A_R^*$  on  $B_I$  for different values of  $C_I$  (here  $B_R = -2$ ,  $C_R = -1$  are fixed; the results also hold for other values of  $B_R$  in the range  $-3 < B_R < -1$ ). We see that  $A_R^*$  is always less than the values of  $A_R$  for which the radial stabilities of the  $u$  solutions are degenerate; thus, if the  $u$  solutions are subcritical then the  $qp$  solutions are also subcritical.

- (iii) Let  $C_I = C'_I$  be fixed, and define  $B'_I$  to be the value of  $B_I$  for which  $(B'_I, C'_I)$  lies on the boundary between regions II and III. If the  $ns$  solutions are supercritical with  $(B_I, C_I) = (B'_I, C'_I)$ , then the  $qp$  solutions will be supercritical for all values of  $(B_I, C_I)$  for which they exist.

Without loss of generality we consider  $B_I < 0$ . Numerical calculations show that  $A_R^*$  is a monotonically decreasing function of  $B_I$  (see Fig. 31); for  $C_I = C_I'$  it reaches its minimum value  $A_{R,\min}^*$  when  $B_I = B_I'$  because for larger values of  $B_I$  the  $qp$  solutions do not exist. For  $(B_I, C_I) = (B_I', C_I')$  the periodic orbit has become a heteroclinic orbit connecting  $ns$  solutions; therefore  $\bar{F}$  is dominated by the  $ns$  solutions so that

$$\bar{G} = F(\theta_{ns}, \phi_{ns}) - 2A_R$$

and hence

$$A_{R,\min}^* = A_R - \frac{1}{2}F(\theta_{ns}, \phi_{ns}).$$

But in this equation  $F(\theta_{ns}, \phi_{ns}) < 0$  because the  $ns$  solutions are supercritical for  $(B_I, C_I) = (B_I', C_I')$ ; thus  $A_{R,\min}^* > A_R$ . But for all other values of  $B_I$  for which  $qp$  solutions exist  $A_R^* > A_{R,\min}^*$  so that  $A_R^* > A_R$ ; therefore the  $qp$  solutions are supercritical.

This leads to the following restrictions on the possible radial stabilities of the solutions. First, we know numerically that if the  $ns$  solutions are supercritical anywhere in region II with  $C_I = C_I'$  they will also be supercritical at  $(B_I, C_I) = (B_I', C_I')$  (see, e.g., Fig. 30(a)); thus, if the  $ns$  and  $qp$  solutions exist and the  $ns$  solutions are supercritical, then the  $qp$  solutions must also be supercritical. Second, if  $A_R, B_R$ , and  $C_R$  have been chosen so that the  $v$  solutions are supercritical, then from (i) the  $ns$  solutions with the same values of these parameters will be supercritical; in particular, they will be supercritical with  $(B_I, C_I) = (B_I', C_I')$  so that the  $qp$  solutions must be supercritical.

- (iv) Suppose that the  $u$  and  $v$  solutions are subcritical, and  $ns$  solutions exist and are supercritical. Then  $qp$  solutions cannot exist.

Consider the value  $A_R = -(B_R + C_R)/2$  for which the radial stability of the  $u$  solution is degenerate; then

$$s_1^{ns} = \frac{B_I + C_I}{B_R C_I - B_I C_R} (|C|^2 - \text{Re}(B\bar{C})).$$

In order for  $ns$  solutions to exist it is necessary that  $|C|^2 - \text{Re}(B\bar{C}) > 0$ . Thus, the curves defined by  $B_I + C_I = 0$  or  $B_R C_I - B_I C_R = 0$  divide the  $(B_I, C_I)$  plane into regions in which  $s_1^{ns}$  is positive or negative (see Fig. 30(b)). Numerically it is seen that  $s_1^{ns} < 0$  only outside of the regions I and II; in other words, if  $ns$  solutions are supercritical then  $qp$  solutions cannot exist. Based on a numerical study of how the curve  $s_1^{ns} = 0$  varies in  $(B_I, C_I)$  space with  $A_R$  (Fig. 30), we conclude that this also cannot happen for larger values of  $A_R$  for which the  $u$  solutions are subcritical.

All possibilities for the radial stability of the  $ns$  and  $qp$  solutions which do not violate the restrictions (i)–(iv) occur for open regions of parameter space with  $-3 < C_R < -1$  and  $C_R = -1$ .

### Appendix C. Proof that heteroclinic cycles involving infinite amplitude solutions are traced out in finite time

Consider a heteroclinic cycle involving the two infinite amplitude fixed points  $A$  and  $B$  as shown in Fig. 32. Near  $B$ , local coordinates are chosen so that

$$\frac{dx_1}{d\tau} = s_3^B x_1, \quad \frac{d\rho}{d\tau} = s_1^B \rho, \quad \frac{dz_1}{d\tau} = s_2^B z_1, \tag{17}$$

where  $s_3^B > 0$ ,  $s_1^B < 0$ , and  $s_2^B < 0$ . Near  $A$ , local coordinates are chosen so that

$$\frac{dx_2}{d\tau} = \alpha x_2 + \beta z_2, \quad \frac{d\rho}{d\tau} = s_1^A \rho, \quad \frac{dz_2}{d\tau} = -\beta x_2 + \alpha z_2, \tag{18}$$

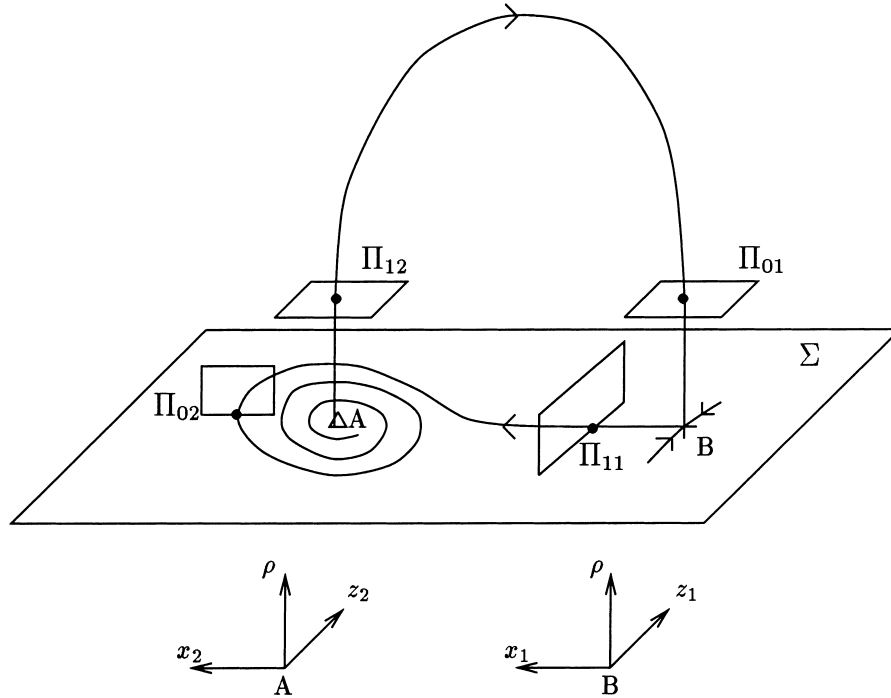


Fig. 32. Heteroclinic cycle involving the *A* and *B* infinite amplitude fixed points. The cross-sections  $\Pi_{01}$ ,  $\Pi_{11}$ ,  $\Pi_{02}$ , and  $\Pi_{12}$  are defined in the text.

where  $\alpha < 0$ ,  $s_1^A > 0$ , and  $\beta > 0$ . As shown in Fig. 32, we construct cross-sections near *B* defined by  $\Pi_{01} \equiv \{\rho = \epsilon\}$  and  $\Pi_{11} \equiv \{x_1 = \epsilon\}$ , and cross-sections near *A* defined by  $\Pi_{02} \equiv \{z_2 = 0\}$  and  $\Pi_{12} \equiv \{\rho = \epsilon\}$ . The parameter  $\epsilon$  is small but finite and is chosen so that the mappings from  $\Pi_{01} \rightarrow \Pi_{11}$  and from  $\Pi_{02} \rightarrow \Pi_{12}$  may be suitably approximated by the linearization of the flow about the fixed points *B* and *A*, respectively. In terms of the time  $\tau$ , the heteroclinic cycle is traced out in infinite time. However, in terms of the original time  $t$  the situation is more subtle because the transformation  $dt/d\tau = \rho$  fails for  $\rho = 0$ ; thus, we consider a limiting procedure in which a trajectory approaches the heteroclinic cycle between the infinite amplitude fixed points. This consists of four parts.

- (i)  $P_{01}^L : \Pi_{01} \rightarrow \Pi_{11}$

Suppose that at  $\tau = 0$  a trajectory passes through  $\Pi_{01}$  with coordinates  $(x_1, \rho, z_1) = (x_{01}, \epsilon, z_{01})$ , with  $x_{01} = z_{01} = 0$  denoting the point on the heteroclinic cycle. From Eq. (17),

$$x_1(\tau) = x_{01} e^{s_3^B \tau}, \quad \rho(\tau) = \epsilon e^{s_1^B \tau}, \quad z_1(\tau) = z_{01} e^{s_2^B \tau}.$$

The time  $\tau$  for the trajectory to go from  $\Pi_{01}$  to  $\Pi_{11}$  (determined by the time required for  $x_1$  to go from  $x_{01}$  to  $\epsilon$ ) is  $\tau = (1/s_3^B)(\log \epsilon/x_{01})$ , a quantity which diverges as  $x_{01} \rightarrow 0$  (i.e., as the heteroclinic cycle is approached). If, however, we work in the original time  $t$  defined by  $dt/d\tau = \rho$ , Eqs. (17) become

$$\frac{dx_1}{dt} = \frac{s_3^B x_1}{\rho}, \quad \frac{d\rho}{dt} = s_1^B, \quad \frac{dz_1}{dt} = \frac{s_2^B z_1}{\rho},$$

with solution

$$x_1(t) = x_{01} \left( \frac{s_1^B t + \epsilon}{\epsilon} \right)^{s_3^B/s_1^B}, \quad \rho(t) = s_1^B t + \epsilon, \quad z_1(t) = z_{01} \left( \frac{s_1^B t + \epsilon}{\epsilon} \right)^{s_2^B/s_1^B}.$$

The time  $t$  to go from  $\Pi_{01}$  to  $\Pi_{11}$  is thus

$$t = \frac{\epsilon}{s_1^B} \left[ \left( \frac{x_{01}}{\epsilon} \right)^{|s_1^B/s_3^B|} - 1 \right].$$

In the limit  $x_{01} \rightarrow 0$  (i.e., as the heteroclinic cycle is approached)  $t \rightarrow \epsilon/|s_1^B|$ , i.e., a *finite* time in the original time variable.

(ii)  $P_{11}^L : \Pi_{11} \rightarrow \Pi_{02}$

Reset time so that at  $\tau = 0$  the trajectory passes through  $\Pi_{11}$  with coordinates  $(x_1, \rho, z_1) = (\epsilon, \rho_{11}, z_{11})$ , with the trajectory on the heteroclinic cycle if  $\rho_{11} = z_{11} = 0$ . Using the time  $\tau$ , it takes a finite time  $T_\tau$  to go from  $\Pi_{11}$  to  $\Pi_{02}$ . Using the time  $t$ , this takes a time

$$T = \int_0^T dt = \int_0^{T_\tau} \rho d\tau \leq \rho_{\max} \int_0^{T_\tau} d\tau = \rho_{\max} T_\tau,$$

where  $\rho_{\max}$  is the maximum  $\rho$  value of the trajectory between  $\Pi_{11}$  and  $\Pi_{02}$ . Thus, since  $T_\tau$  is finite, so is  $T$ . In fact,  $\rho_{\max} \rightarrow 0$  in the limit  $\rho_{11} \rightarrow 0, z_{11} \rightarrow 0$ ; thus, in the limit as the trajectory approaches the heteroclinic cycle, the time of flight from  $\Pi_{11}$  to  $\Pi_{02}$  is *zero* in the original time variable.

(iii)  $P_{02}^L : \Pi_{02} \rightarrow \Pi_{12}$

We now reset time so that at  $\tau = 0$  the trajectory passes through  $\Pi_{02}$  with coordinates  $(x_2, \rho, z_2) = (x_{02}, \rho_{02}, 0)$  chosen such that the heteroclinic cycle forms when  $\rho_{02} = 0$  and  $x_{02}$  takes an appropriate value. From Eq. (18),  $\rho(\tau) = \rho_{02} e^{s_1^A \tau}$ . The time  $\tau$  for the trajectory to go from  $\Pi_{02}$  to  $\Pi_{12}$  (determined by the time required for  $\rho$  to go from  $\rho_{02}$  to  $\epsilon$ ) is  $\tau = (1/s_1^A)(\log \epsilon/\rho_{02})$  which diverges as  $\rho_{02} \rightarrow 0$ . If, however, we work in the original time  $t$ , then  $d\rho/dt = s_1^A$  with solution  $\rho(t) = s_1^A t + \rho_{02}$ . The time  $t$  to go from  $\Pi_{02}$  to  $\Pi_{12}$  is thus  $t = (\epsilon - \rho_{02})/s_1^A$ . In the limit  $\rho_{02} \rightarrow 0$  (i.e., as the heteroclinic cycle is approached)  $t \rightarrow \epsilon/s_1^A$ , a *finite* time in the original time variable.

(iv)  $P_{12}^L : \Pi_{12} \rightarrow \Pi_{01}$

Using the time  $\tau$ , it takes a finite time  $T_\tau$  to go from  $\Pi_{12}$  to  $\Pi_{01}$ . As for case (ii), using the time  $t$  this takes a time  $T \leq \rho_{\max} T_\tau$  where  $\rho_{\max}$  is the maximum  $\rho$  value of the trajectory between  $\Pi_{12}$  and  $\Pi_{01}$ . Since  $T_\tau$  is finite, so is  $T$ .

Since each part of the heteroclinic cycle is traced out in finite or zero time the whole cycle is traced out in finite time. A similar argument holds for heteroclinic cycles involving an infinite amplitude limit cycle.

## References

- [1] R. Lauterbach, M. Roberts, Heteroclinic cycles in dynamical systems with broken spherical symmetry, J. Diff. Eq. 100 (1992) 22–48.
- [2] E. Knobloch, System symmetry breaking and Shil'nikov Dynamics, in: J. Chadam, M. Golubitsky, W. Langford, B. Wetton (Eds.), Pattern Formation: Symmetry Methods and Applications, American Mathematical Society, Providence, 1996, pp. 271–279.
- [3] P. Hirschberg, E. Knobloch, Complex dynamics in the Hopf bifurcation with broken translation symmetry, Physica D 92 (1996) 56–78.
- [4] J.D. Crawford, E. Knobloch, Symmetry and symmetry-breaking bifurcations in fluid mechanics, Ann. Rev. Fluid Mech. 23 (1991) 341–387.
- [5] M. Golubitsky, I. Stewart, D.G. Schaeffer, Singularities and Groups in Bifurcation Theory, vol. II, Springer, New York, 1988.
- [6] T. Clune, E. Knobloch, Mean flow suppression by endwalls in oscillatory binary fluid convection, Physica D 61 (1992) 106–112.
- [7] A.D.D. Craik, I.M. Moroz, Temporal evolution of interaction waves in non-conservative systems: some exact solutions, Wave Motion 10 (1988) 443–452.
- [8] E. Knobloch, J. Moehlis, Bursting mechanisms for hydrodynamical systems, in: M. Golubitsky, D. Luss, S.H. Strogatz (Eds.), Pattern Formation in Continuous and Coupled Systems, Springer, New York, 1999, pp. 157–174.
- [9] E. Knobloch, J. Moehlis, Burst mechanisms in hydrodynamics, in: L. Debnath, D. Riahi (Eds), Nonlinear Instability, Chaos, and Turbulence, vol. II, Computational Mechanics Publications, Southampton, in press.
- [10] J.W. Swift, Hopf bifurcation with the symmetry of the square, Nonlinearity 1 (1988) 333–377.
- [11] A.S. Landsberg, E. Knobloch, Oscillatory bifurcation with broken translation symmetry, Phys. Rev. E 53 (1996) 3579–3600.

- [12] J. Moehlis, E. Knobloch, Forced symmetry breaking as a mechanism for bursting, *Phys. Rev. Lett.* 80 (1998) 5329–5332.
- [13] G. Dangelmayr, E. Knobloch, Hopf bifurcation with broken circular symmetry, *Nonlinearity* 4 (1991) 399–427.
- [14] S.A. van Gils, M. Silber, On the uniqueness of invariant tori in  $D_4 \times S^1$  symmetric systems, *Nonlinearity* 8 (1995) 615–628.
- [15] T. Clune, E. Knobloch, Pattern selection in three-dimensional magnetoconvection, *Physica D* 74 (1994) 151–176.
- [16] X.M. Gu, P.R. Sethna, Resonant surface waves and chaotic phenomena, *J. Fluid Mech.* 183 (1987) 543–565.
- [17] Z.C. Feng, P.R. Sethna, Symmetry-breaking bifurcations in resonant surface waves, *J. Fluid Mech.* 199 (1989) 495–518.
- [18] I. Melbourne, P. Chossat, M. Golubitsky, Heteroclinic cycles involving periodic solutions in mode interactions with  $O(2)$  symmetry, *Proc. Roy. Soc. Edinburgh A* 113 (1989) 315–345.
- [19] C. Tresser, About some theorems by L.P. Shil'nikov, *Ann. Inst. Henri Poincaré* 40 (1984) 441–461.
- [20] S. Wiggins, *Global Bifurcations and Chaos*, Springer, New York, 1988.
- [21] P. Hirschberg, E. Knobloch, Shil'nikov–Hopf bifurcation, *Physica D* 62 (1993) 202–216.
- [22] P. Glendinning, C. Sparrow, Local and global behavior near homoclinic orbits, *J. Stat. Phys.* 35 (1984) 645–695.
- [23] J.W. Swift, K. Wiesenfeld, Suppression of period doubling in symmetric systems, *Phys. Rev. Lett.* 52 (1984) 705–708.
- [24] E. Knobloch, N.O. Weiss, Bifurcations in a model of double-diffusive convection, *Phys. Lett. A* 85 (1981) 127–130.
- [25] C.T. Sparrow, *The Lorenz Equations: Bifurcations, Chaos, and Strange Attractors*, Springer, New York, 1982.
- [26] A. Back, J. Guckenheimer, M.R. Myers, F.J. Wicklin, P.A. Worfolk, *dstool: Computer assisted exploration of dynamical systems*, *Not. Am. Math. Soc.* 39 (1992) 303–309.
- [27] E. Doedel, A. Champneys, T. Fairgrieve, Y. Kuznetsov, B. Sandstede, X. Wang, *AUTO 97: Continuation and bifurcation software for ordinary differential equations* (available via FTP from directory pub/doedel/auto at ftp.cs.concordia.ca) (1997).
- [28] P. Chossat, M. Golubitsky, Symmetry-increasing bifurcation of chaotic attractors, *Physica D* 32 (1988) 423–436.
- [29] J.D. Rodriguez, M. Schell, Global bifurcations into chaos in systems with  $SO(2)$  symmetry, *Phys. Lett. A* 146 (1990) 25–31.
- [30] A.C. Newell, D.A. Rand, D. Russell, Turbulent dissipation rates and the random occurrence of coherent events, *Phys. Lett. A* 132 (1988) 112–123.
- [31] A.C. Newell, D.A. Rand, D. Russell, Turbulent transport and the random occurrence of coherent events, *Physica D* 33 (1988) 281–303.
- [32] E. Knobloch, D.R. Moore, Minimal model of binary fluid convection, *Phys. Rev. A* 42 (1990) 4693–4709.
- [33] E. Knobloch, D.R. Moore, Chaotic travelling wave convection, *Eur. J. Mech. B/Fluids* 10(2, suppl.) (1991) 37–42.
- [34] N. Platt, E.A. Spiegel, C. Tresser, On-off intermittency: a mechanism for bursting, *Phys. Rev. Lett.* 70 (1993) 279–282.
- [35] P. Ashwin, E. Covas, R. Tavakol, Transverse instability for non-normal parameters, *Nonlinearity* 12 (1999) 563–577.
- [36] D. Armbruster, Codimension 2 bifurcation in binary convection with square symmetry, in: F.H. Busse, L. Kramer (Eds.), *Nonlinear Evolution of Spatio-Temporal Structures in Dissipative Continuous Systems*, Plenum Press, New York, 1990, pp. 385–398.
- [37] D. Armbruster, Square and almost square symmetry in binary convection, *Eur. J. Mech. B/Fluids* 10(2, suppl.) (1991) 7–12.
- [38] P. Ashwin, Z. Mei, Normal form for Hopf bifurcation of partial differential equations on the square, *Nonlinearity* 8 (1995) 715–734.
- [39] M. Golubitsky, I.N. Stewart, Hopf bifurcation with dihedral group symmetry, in: *Multiparameter Bifurcation Theory*, Contemporary Maths, vol. 56, American Mathematical Society, Providence, 1986, pp. 131–173.
- [40] P. Ashwin, P. Stork, Permissible symmetries of coupled cell networks, *Math. Proc. Camb. Phil. Soc.* 116 (1994) 27–36.
- [41] A. Steindl, H. Troger, One and two-parameter bifurcations to divergence and flutter in the three-dimensional motions of a fluid conveying viscoelastic tube with  $D_4$  symmetry, *Nonlinear Dyn.* 8 (1995) 161–178.
- [42] T.S. Sullivan, G. Ahlers, Nonperiodic time dependence at the onset of convection in a binary liquid mixture, *Phys. Rev. A* 38 (1988) 3143–3146.
- [43] F. Simonelli, J.P. Gollub, Surface wave mode interactions: effects of symmetry and degeneracy, *J. Fluid Mech.* 199 (1989) 471–494.
- [44] E. Knobloch, A.S. Landsberg, A new model of the solar cycle, *Mon. Not. Roy. Astr. Soc.* 278 (1996) 294–302.
- [45] E. Knobloch, S.M. Tobias, N.O. Weiss, Modulation and symmetry changes in stellar dynamos, *Mon. Not. Roy. Astr. Soc.* 297 (1998) 1123–1138.
- [46] P. Ashwin, G. Dangelmayr, I. Stewart, M. Wegelin, Oscillator networks with the symmetry of the unit quaternion group, in: P. Chossat (Ed.), *Dynamics, Bifurcation and Symmetry*, Kluwer Academic Publishers, Dordrecht, 1994, pp. 35–48.